NTNU

Norwegian University of
Science and Technology

Applications of screw extrusion for pure aluminium and aluminium foils

Martin Storli Værnes

Materials Science and Engineering (MTMT)
Submission date: July 2018
Supervisor: Hans Jørgen Roven, IMA
Co-supervisor: Trond Furu, IMA
Oddvin Reiso, IMA

Norwegian University of Science and Technology
Department of Materials Science and Engineering

Preface

This master's thesis is written at NTNU-Department of Materials Science and Engineering, during spring 2018. The thesis is a result of collaboration between Hydro and NTNU to improve aluminium recycling. I hereby declare that this master's thesis has been done independently and in accordance with regulations at NTNU.

Trondheim, 2018-07-02

Martin Storli Værnes

Digitalt signert av Martin Storli Værnes
DN: cn=Martin Storli Værnes, o=NTNU, ou=Institutt for materialteknologi, email=martin-sv@hotmail.com, c=NO
Dato: 2018.07.02 22:47:53 +02'00'

Martin Storli Værnes

Acknowledgment

I would like to thank my supervisor Professor Hans Jørgen Roven and my co-supervisors, Adjunct Professor Oddvin Reiso and Adjunct Professor Trond Furu for valuable advise during the work with this master thesis.

I would also like to thank Senior Engineer Pål Skaret for help with mechanical testing, Senior Engineer Trygve Schanche for guidance with metallographic work and Yingda Yu for assistance with SEM-imaging. I would also like to thank Master's Student Hans Sigurd Amundsen, Dr. Kristian Grøtta Skorpen and PhD-candidate Geir Langelandsvik for their contribution to the experimental work with the screw extrusion prototype.

(MSV)

Aim of work

This master's thesis aims to investigate possible applications for screw extruded products that can reduce energy use and environmental cost for recycled aluminium. Two applications are assessed: (i) screw extrusion to produce electrically conducting wires, and (ii) screw extrusion as a compacting technique to easier remelt scrap.

99.99% pure aluminium was chosen to assess the effect of screw extrusion on electrical conductivity and mechanical properties of aluminium. The electrical conductivity of super pure aluminium is referenced in literature, and can be compared to screw extruded wires. Super pure aluminium contains a low amount of foreign elements, so the effect of the unique microstructure and increased oxide content typical of screw extruded profiles can then be evaluated without the results being effected by impurities.

Commercial purity aluminium foils were chosen as feedstock for screw extrusion, since foil materials face challenges in recycling operations. Aluminium foil is widely used in households today, but recycling can be difficult due to low thickness and contamination of organic products. Screw extrusion has never been successfully tested with aluminium foil as feedstock. Due to the large surface area of foils, delamination after compacting and extrusion could be a problem.

Abstract

This thesis has assessed the effect of the screw extrusion process for electrical conductivity on a super pure aluminium Ø 3mm wire. This thesis also tested if commercial quality aluminium foil could be screw extruded into a product with metallic bonding.

The electrical conductivity of screw extruded 3mm wires were tested and showed a minimal decrease in conductivity for the super pure aluminium compared to values found in literature. The conductivity for the aluminium foil based Ø 3mm wire was much lower mainly due to the high iron content.

The mechanical properties of screw extruded aluminium foil based products were good due to a high iron content and good metallic bonding. The screw extruded aluminium foil based 10mm profile showed similar mechanical properties to the 3mm wire. The average density of compacted foil is over 97%. The screw extruded aluminium foil shows promising results for easier recycling of materials with a high surface to volume ratio.

Sammendrag

I denne masteroppgaven ble effekten av skrueekstrudering på elektrisk ledningsevne av en Ø 3mm tråd laget av 99,99% superrent aluminium(SP-Al). Det ble også forsøkt å skrueekstrudere kommersielt ren aluminiumsfolie til en tråd på 3mm, og en stang på 10mm.

Den elektriske ledningsevnen til skrueekstrudert SP-Al ble målt og viste en litt lavere verdi enn verdier funnet i faglitteraturen. Den elektriske ledningsevnen til skrueekstrudert aluminiumsfolie Ø 3mm tråd var mye lavere hovedsakelig grunnet høyt jerninnhold.

De mekaniske egenskapene til skrueekstrudert aluminiumsfolie var gode, hovedsakelig grunnet av høyt jerninnhold og god metallisk kontakt. De mekaniske egenskapene var relativt like for den skrueekstruderte stangen og den skrueekstruderte tråden som begge var laget av aluminiumsfolie. Den gjennomsnittlige tettheten til de skrueekstruderte aluminiumsfoliene var over 97%. Å skrueekstrudere aluminiumsfolie ga lovende resultater for å enklere resirkulere materialer med stor overflate i forhold til volum.

Contents

1 Introduction

Conventional recycling of aluminium only consumes 5% of the energy compared to creating new primary aluminium from raw ore [1]. A new method for recycling aluminium scrap has been developed by NTNU and Hydro[2] and is named screw extrusion. The method works by compressing aluminium scrap using the pressure generated by a screw, combined with elevated temperature. This thesis aims to improve recycling of aluminium scrap in a cost effective way using screw extrusion.

Two applications are evaluated for the screw extrusion process. The first application is recycling aluminium scrap into 3mm electrical conducting aluminium wires. The second application is compacting low thickness aluminium foils into a bulk product.

Aluminium conductors are extensively used in the high voltage conduction market, due to their low price and high conductivity to weight ratio[3]. Power transfer lines span large distances carrying high voltage. The weight of the cable limits the distance between each pylon, and therefore aluminium with its low weight is preferred. For low voltage conduction, copper conductors are chosen due to better fatigue properties and a high conductivity to diameter ratio. The low voltage conduction market is mostly made up of electrical wires for household applications. By utilizing screw extruded wires, the costs of producing conducting aluminium wires can be reduced. This could increase the market share of aluminium conductors for the low voltage conductor market.

Thin sheets of aluminium and aluminium foils are hard to recycle, due to their low thickness[4] and high surface to volume ratio. Using traditional remelting techniques aluminium oxides are formed and a lower metal yield is achieved. If screw extrusion could compact the foil before remelting, oxidizing can be reduced and large energy savings can be made.

2 | Theory

2.1 Solid-state recycling

Potential "meltless" paths for recycling aluminium have achieved attention due to even less energy use and environmental impact compared to conventional recycling by remelting. These include the NTNU and Norsk Hydro patented screw extrusion process. The energy use for three different solid state recycling techniques has been calculated by Duflou et al.[5] and compared to traditional remelting. The result gives an average energy use of 0.35 kWh/kg[5] for screw extrusion versus 0,69 kWh/kg[6] (converted from Joule to kWh) for a state of the art remelting furnace. For a conventional recycling path the material must be extruded after remelting, requiring even more energy.

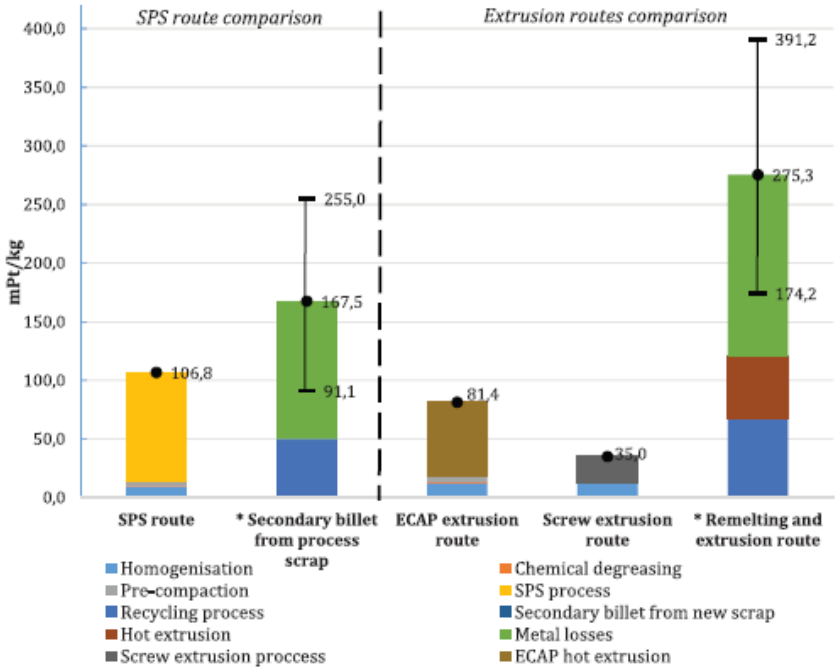

Figure 2.1: Sketch of the environmental impact of different recycling routes for aluminium scrap. From [5].

The environmental impact, measured in mPt (a measure of annual environmental load[7]) can be seen in figure 2.1. The large variation for the remelting and extrusion route in figure 2.1 is due to different rates of oxide creation during processing and remelting. Aluminium oxide formed during remelting removes aluminium metal from the melt and reduced yield.

2.1.1 Scrap sorting

Scrapped components containing aluminium metal often also contains many other elements such as iron, copper and Magnesium, or plastics. The main sorting categories include separating metals from non-metals and ferrous metals from non-ferrous metals. Some methods key separation methods for recycling can be seen in Table 2.1 below.

Table 2.1: Separation methods for recycling of aluminium. From [8].

Desired separation	Separation method **
Metal - non-metal	
Steel from non-metal + non-magnetic metal	Drum magnet, overbelt magnet
Nonmagnetic metal from non-metal	Screen, air elutriator, eddy current rotor, eddy current coil sensor
Metal from non-metal fines (<9mm)	Jig, eddy current rotor
Non-metal or other metal contaminants from A1	Magnetic headpulley, eddy current rotor, hand sort
Al - other metal	
Light from dense NF metals	Sink-float (wet or dry), eddy current rotor
Mg from Al	hand sorting, colour sensor, XRT sensor
Other metal contaminants from Al	
Al - A1	
Al with attachments from liberated Al	Hand sorting, XRT sensor
Bare from painted or dirty Al	Hand sorting, colour sensor
Alloy grouping & Al by alloy	LIBS sensor, XRF sensor
Particle-by-particle target alloy batching	LIBS sensor, XRF sensor
Average particle stream elemental composition measurement	LIBS sensor, XRF sensor, PGNAA sensor

** LIBS = Laser–Induced Breakdown Spectroscopy; XRF = X-Ray Fluorescence; XRT = X-Ray Transmission; PGNAA = Prompt Gamma Neutron Activation Analysis

Pure primary aluminium needs to be added to the recycled melt to reduce the total alloy content of the melt[8] if the alloying elements are not sorted or refined out.

2.1.2 Aluminium foils

Aluminium foils, and thin aluminium sheets face challenges in recycling. The low thickness of aluminium foils/sheets and large surface area to volume creates large amount of surface oxide if the foil is heated with access to oxygen. Aluminium oxide forms before and during melting, leading to large metal losses[5]. This reduces the metal yield of aluminium from the melt.

Another issue is that aluminium foil can be tainted with leftover food and stains. Thin sheets used on the inside of food containers is often hard to separate from the food containers. If this scrap is tossed straight into an aluminium melt the melt can be contaminated. Figure 2.2 shows that dirty foil is one of the most difficult materials to recycle.

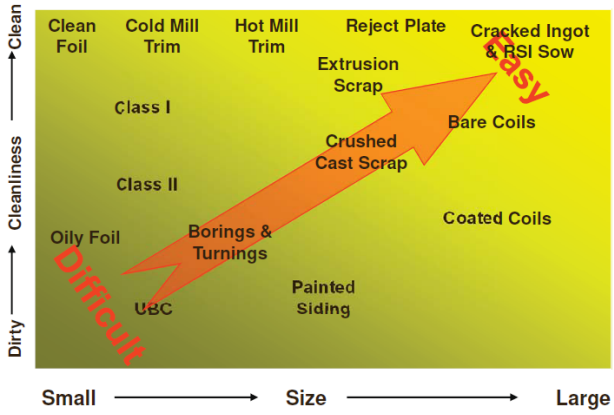

Figure 2.2: Complexity of recycling different types of scrap. From [4].

Aluminium from household applications follows the general garbage disposal route and is combusted at 850°C[9]. The aluminium is then found at the bottom of the furnace, either as contaminated aluminium oxide or as remelted aluminium. This is not refined and needs refining or remelting to go back into the aluminium life-cycle[8].

Aluminium foils that are collected by scrap metal dealers are sold in bulk according to the scrap grade. The American Institute of Scrap Recycling Industries(ISRI) has standardized scrap specifications for different foils. Three code names are used; (i) Terse - for new aluminium foil, (ii) Tesla - for post-consumer aluminium foil and (iii) Tetra - for new coated aluminium foil[10].

2.2 Screw extrusion

2.2.1 General description

Screw extrusion is a continuous extrusion process developed and patented by NTNU and Hydro. The process works by compacting scrap granulates using a screw against a chamber and a die. A sketch of the screw extrusion chamber is presented in figure 2.3. The scrap granulates enters the screw in section A in figure 2.3, and moves forward with the rotation of the screw. In section C scrap will build up, and compact into a solid bulk. This is then extruded out of the extrusion die hole.

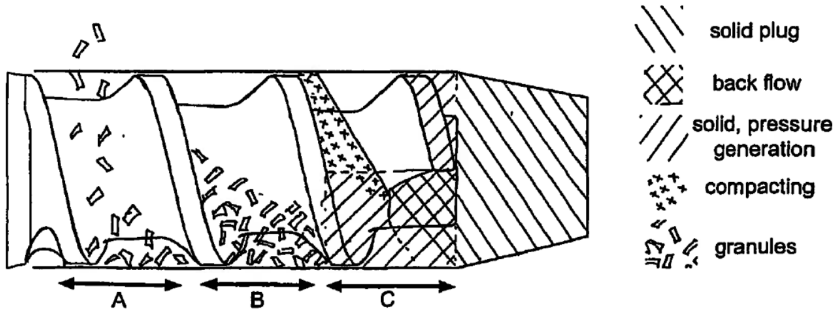

Figure 2.3: Sketch of the screw extruder prototype chamber with granules(feedstock) entering the rear in A. In section C, the granules compacts into a solid bulk. From [2].

2.2.2 Influence of flow stress

The flow stress is the stress required to plastically deform a metal. To compact granules into a solid bulk, the screw rotation must overcome the flow stress of the granules. As seen in figure 2.4 the flow stress is heavily influenced by the temperature of the work piece. By heating the workpiece to 400-500°C the flow stress can be reduced as much as five- or tenfold[11]. For screw extrusion the reduction in flow stress is of great importance to the screw momentum. Alloys with high flow stress would not be possible to extrude without lowering the flow stress with temperature. If the temperature is too high, the scrap may melt inside the extruder. This could lead to material flowing outside the chamber and damaging the extruder. Therefore tempera-

ture control is important for screw extrusion.

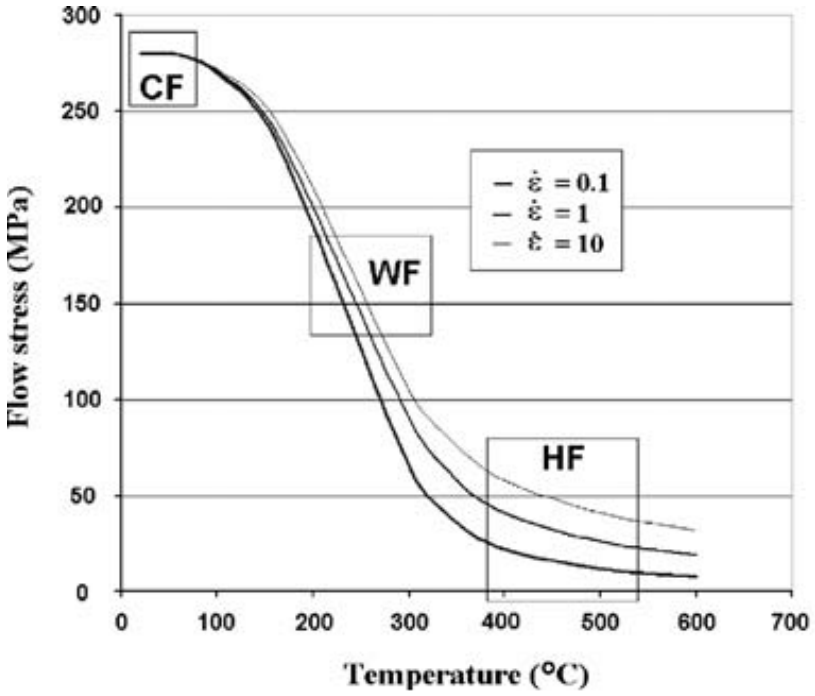

Figure 2.4: Temperature dependence of flow stress for three strain rates for a typical, unspecified Al-alloy. CF means Cold Forming, WF means Warm Forming and HF means Hot Forming. From [11].

2.2.3 Aluminium oxide formation

On the surface of aluminium in contact with air a thin layer of aluminium oxide is formed. This thin layer is about 2-4nm thick[12] and gives aluminium its good corrosion properties[13]. The thickness of the oxide layer depends on the temperature and aging time[14]. During screw extrusion the surface oxide is broken down when granules are compacted and oxides are enclosed in the bulk of the material. During screw extrusion aluminium oxide is also formed due to oxygen inside the extruder reacting with deformed aluminium granules[15]. The increased amount of aluminium oxide in the bulk of a screw extruded profile can give a strength contribution if they are of sufficient volume.

2.3 Electrical conductivity

2.3.1 General considerations

The electrical conductivity of a material describes the ease of transferring electrons through its structure. There are three major groups of classifying electrical conductivity, conductors, semiconductors and insulators.

Electrical conductors include most elements with metal bonding. Pure metals give better conductivity than alloys mainly due to less distortions in the lattice structure. Semiconductors includes semi-metals such as Silicon, and have lower conductivity. These are not used as conductors without being altered first. Insulators are non-conducting materials, so no electron transport will occur.

The mechanisms behind conductivity can be simplified by looking at the band structure of the material. Figure 2.5 shows the difference between the valence band and the conduction band for different types of conductors. If the valence band and the conduction band does not overlap, there is an energy difference between the bands, and electrons needs to be in an excited state to conduct electricity. Insulators has a very large band gap, and a large amount of energy is needed to excite atoms to conduct electricity.

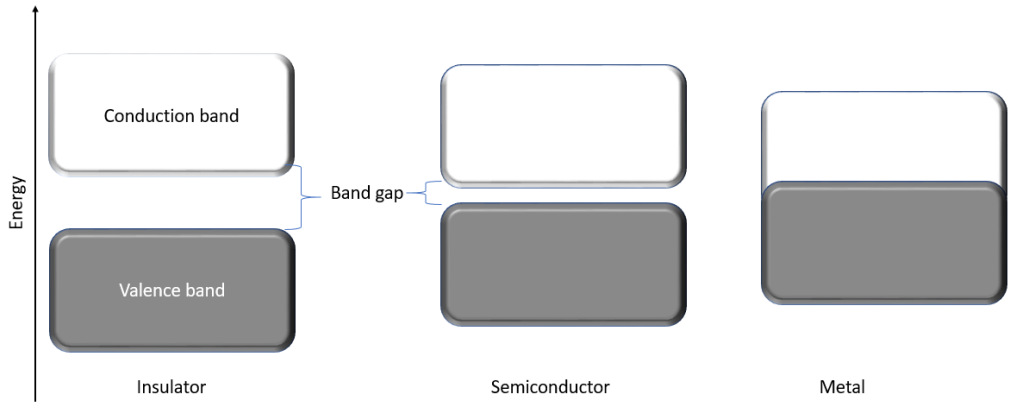

Figure 2.5: Sketch of the band gap for three groups of materials. Made by author.

The temperature of a material will affect its conductivity. For metals an increase in temperature will give a decreased conductivity, while for a semiconductor an increase in temperature will give an increased conductivity.

2.3.2 Relation between resistance, resistivity and conductivity

The electrical resistance, R[Ω] expresses the electrical resistance in a circuit, and is widely used when looking at the resistance in a system. It represents the total resistance in the system, independent of size. The electrical resistivity, ρ[Ω m] is a measure for the resistance times length and is used when comparing different materials on electrical resistivity. The relation between electrical resistance R and electrical resistivity ρ can be seen in equation 2.1. A is the cross-sectional area of the sample, and L is the length of the sample. If a 4-point probe test is used, the L is the distance between measuring points for the voltage.

$$R = \frac{L * \rho}{A} \tag{2.1}$$

The electrical resistivity ρ is the inverse of the electrical conductivity σ, and is given by equation 2.2.

$$\sigma = \frac{1}{\rho} \tag{2.2}$$

The electrical conductivity is measured in Siemens per meter, where Siemens (S) is the inverse of ohm (Ω). For practical reasons, the electrical conductivity of metals is usually given in Mega Siemens per metre. For a wire we can use equation 2.3 to find the conductivity using the cross-sectional area A, and the length between the voltage measuring points L. If the density, mass and length of the sample is used instead of the area, we get the equation 2.4. The new l is the length of the sample, ρ_d is the density of the sample and m is the mass.

$$\sigma = \frac{L}{A * R} \tag{2.3}$$

$$\sigma = \frac{L * l * \rho_d}{R * m} \tag{2.4}$$

The conductivity can also be expressed as a percentage of the conductivity of copper, known as the International Annealed Copper Standard (% IACS). This sets the electrical conductivity of commercial pure annealed copper to 58 MS/m at 20°C and then the electrical conductivity (σ) can be calculated in % IACS from MS/m through the equation 2.5 [16]:

$$\%IACS\ for\ material\ x = \frac{x\frac{MS}{m}}{58\frac{MS}{m}} * 100\% \tag{2.5}$$

2.3.3 Effect of impurities and defects on electrical conductivity

The conductivity of a material is dependent on several factors that can occur naturally or be introduced during manufacture. Foreign elements are widely used to enhance the mechanical properties of a material by creating deformations in the lattice, this will however also decrease the electrical conductivity[17]. The effect on the electrical conductivity is heavily dependent on how the foreign elements are arranged, in solid solution or precipitated out[15]. Deformation and grain boundaries can also affect the conductivity, figure 2.6 shows an imagined path of an electron through a metal lattice that contains vacancies, foreign elements and grain boundaries.

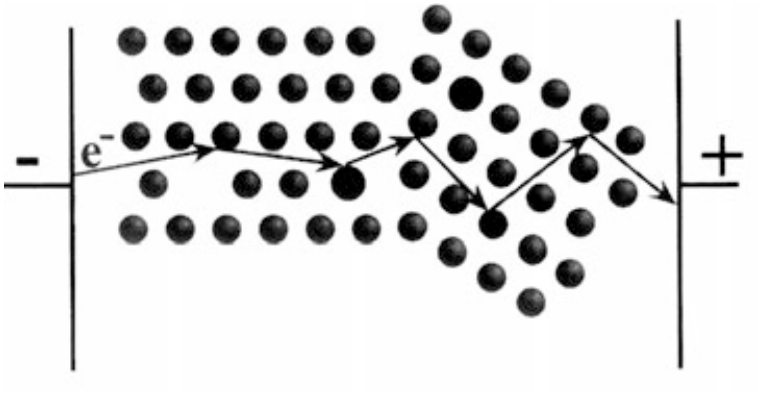

Figure 2.6: Sketch of an imagined electron path. From [18]

2.3.4 The effect of deformation on electrical conductivity

The effect of deformation on the electrical conductivity of metals has been experimentally determined by Schrank et al. and the results show that the resistivity increases steeply from 0 to 30% deformation with a 3% increase in resistivity at 30% deformation for a pure aluminium sample. Then the increase in resistivity is linear until about 98% deformation where the resistivity no longer increases. This can be seen in figure 2.7. At 98% deformation, the resistivity is increased by about 10% [19].

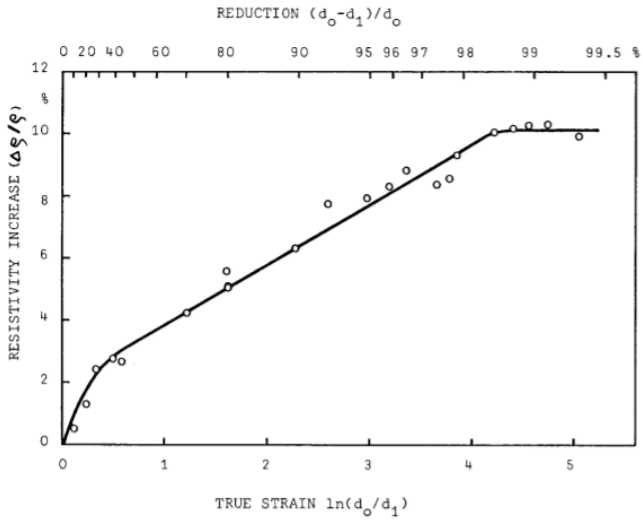

Figure 2.7: The effect of deformation strain on resistivity on a pure aluminium sample. From [19].

2.3.5 Matthiessen's rule

Matthiessen's rule states that the total resistivity of a material can be divided into several independent resistivities. These individual resistivities are divided in to thermal and residual resistivities, and can be added up to find the total resistivity as seen in equation 2.6.

$$\rho_{\text{total}} = \rho_{\text{thermal}} + \rho_{\text{residual}} = \rho_{\text{thermal}} + \rho_{\text{impurities}} + \rho_{\text{defects}} \tag{2.6}$$

Under certain conditions the individual resistances are not independent of each other, and this is named deviations from Matthiessen's rule, and is documented in literature (Seth and Woods[20]).

The addition of alloying elements has been experimentally tested by (Hummel[18]) and can be seen in figure 2.8. The resistivity is increased for increased nickel content in a copper metal, and the figure also shows that increased temperature also increases the resistivity.

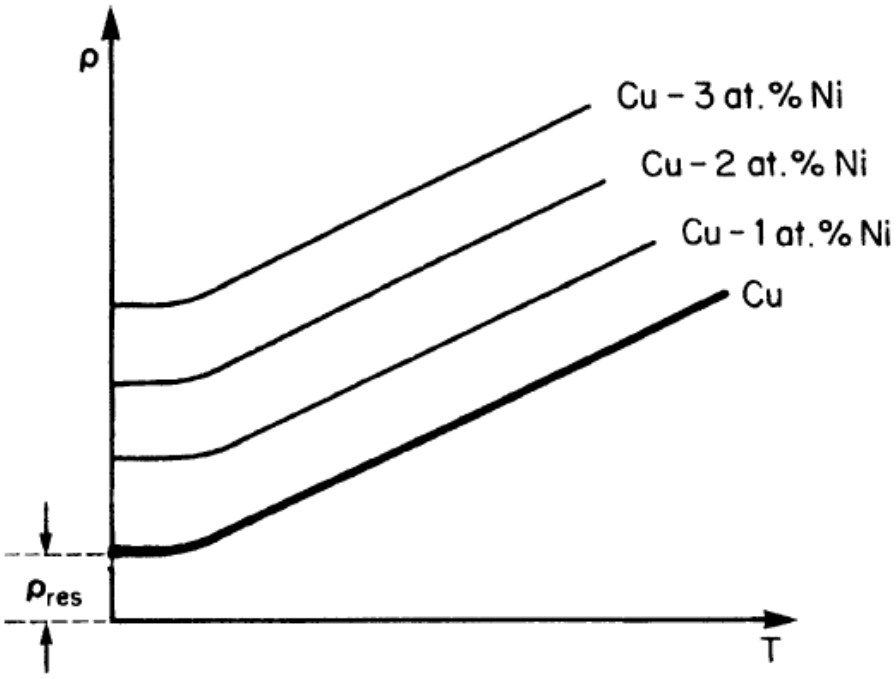

Figure 2.8: The effect of alloying content of nickel on resistivity for copper. From [18].

2.3.6 Effect of alloying elements in solid solution or as precipitates

Alloying elements or impurities can either be a part of the crystal structure as solid solution, or precipitate out as particles that are not part of the crystal lattice. For elements in solid solution a strain field is created that hinders dislocation glide and scatters electrons[21]. This decreases the conductivity, but also increases tensile strength. If the foreign elements are precipitated out as particles, they do not reduce the conductivity as much. This has been experimentally determined for Iron in a pure Aluminium alloy ([15]). Some elements are more detrimental than others for conductivity, and figure 2.9 shows the effect for a selection of elements that can be present in an aluminium alloy[22].

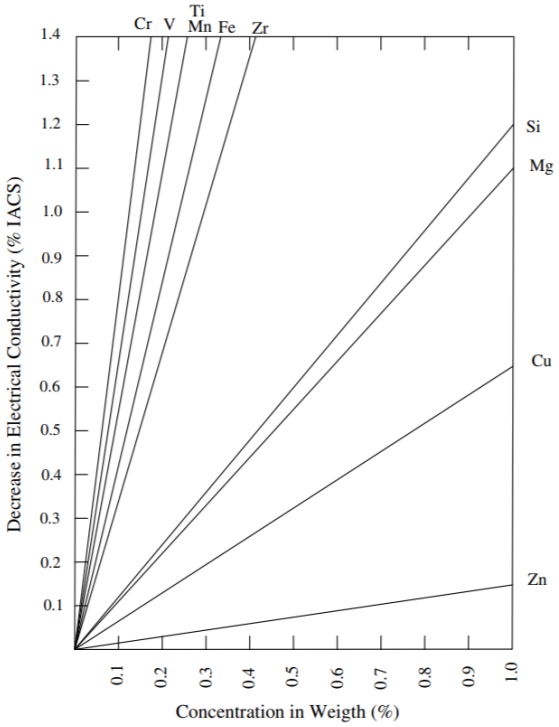

Figure 2.9: The effect of alloying elements on conductivity for aluminium. From [22].

The effect of some alloying elements on electrical resistivity is presented in table 2.2. The increase in resistivity is higher for all elements in solution.

Table 2.2: The effect of some alloying elements on electrical resistivity for aluminium in solution or out of solution. Modified table from[17].

Element	Maximum solubility in Aluminium, %	Average increase in resistivity in solution per wt% [microohm-cm]	Average increase in resistivity out of solution per wt% [microohm-cm]
Iron	0.052	2.56	0.058
Manganese	1.82	2.94	0.34
Silicon	1.65	1.02	0.088
Copper	5.65	0.344	0.030
Magnesium	14.9	0.54 (up to 10%)	0.22
Nickel	0.05	0.81	0.061
Titanium	1	2.88	0.12

To reduce the amount of elements in solid solution it is favourable to have them eliminated from the melt by adding chemical agents, or precipitated during aging. Precipitation of sufficient size will reduce the distortions in the lattice and increase conductivity[23].

2.4 Heat treatment & kinetics

2.4.1 Al-Fe phase diagram

Iron is a common alloying element for low-alloyed aluminium to increase strength. The solubility of iron in aluminium is only about 1% at 650°C as seen in figure 2.10. This implicates that almost all Iron in an aluminium alloy (commercial with less than 5% Fe) will be in the form of precipitates. For Iron to be able to go in to solid solution a temperature of at least 550°C is needed. As phase diagrams assume equilibrium conditions, the reality of iron precipitation is not always like this. To account for this one can use a TTT-diagram.

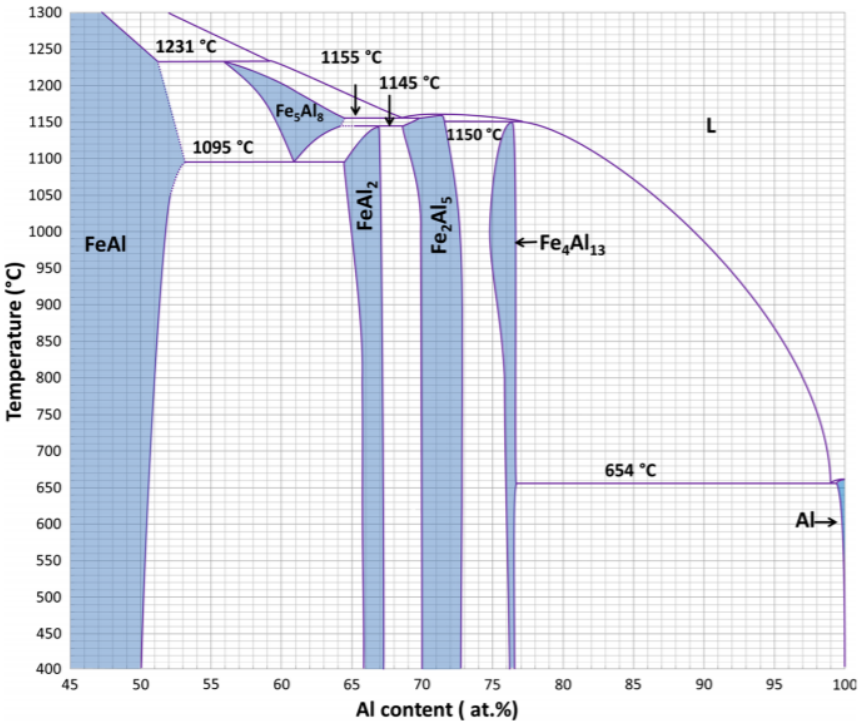

Figure 2.10: Al-rich part of binary phase diagram for Al-Fe. From [15].

2.4.2 Precipitation of Fe

A Time-Temperature-Transformation diagram (TTT-diagram) displays how the microstructure develops for a given temperature-time course. For precipitation of ferrous particles in a pure aluminium alloy precipitation occurs the fastest at 450°C and this can be seen in figure 2.11. Precipitation of iron in aluminium is slow, as for the fastest temperature (450°C) precipitation is finished after 20 hours. This implies that for traditionally cooled aluminium alloys, some iron could be stuck in solid solution even at room temperature.

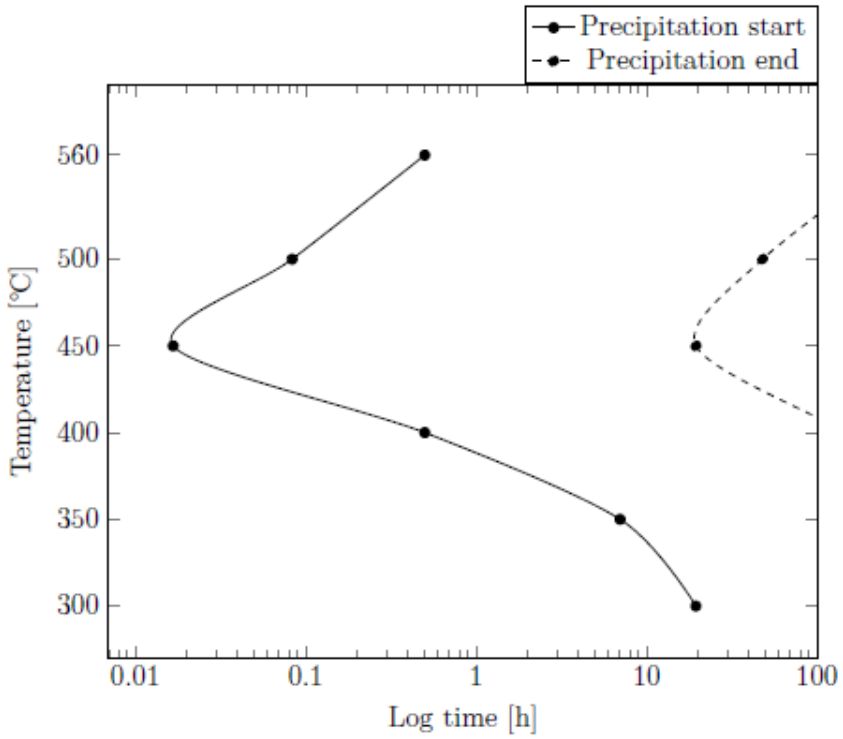

Figure 2.11: Time-Temperature-Transformation diagram for precipitation of Iron in aluminium. From [15].

2.4.3 Recrystallization

Deformation is an effective way of increasing the strength of a metal, due to the buildup of stacking fault energy. Thermodynamics state that some microstructural orientations are the most energetically favourable for given metals, those that minimize stacking fault energy. One could expect that a deformed metal would spontaneously rearrange itself back to an un-deformed state (named recrystallization) to reduce its stacking fault energy, yet this does not happen in practise[24].

To explain this one must include kinetics. A deformed metal must have sufficient energy to overcome the activation energy to change structure. This activation energy is highly dependent on the temperature of the metal, so whether a metal will reorient itself (recrystallize) is heavily dependent on its temperature. Figure 2.12 shows how the Yield strength of three different aluminium alloys used for aluminium foils changes with annealing temperature. As screw extrusion is performed at elevated temperatures, the possibility of recrystallization is important to consider when trying to optimize mechanical properties.

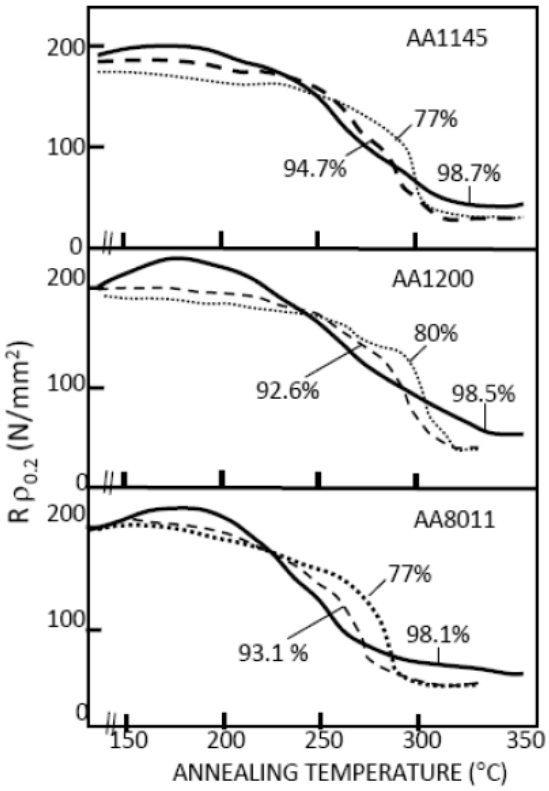

Figure 2.12: Change in Yield stress for different annealing temperatures. From [25].

2.4.4 Concurrent precipitation

Precipitated elements can disturb normal recrystallization of metals. If precipitation occurs at the same time and temperature as recrystallization, recrystallization can be delayed significantly. This delay can be as large as 500x and occurs due to precipitates pinning the grain boundaries and hinder their movement[26].

3 | Experimental procedure

3.1 Base materials

The base material feedstock that was used for screw extrusion in this thesis is shown in figure 3.1. The granulated aluminium foil is shown to the left and a super pure (99.99%) Vigeland cube is shown to the right.

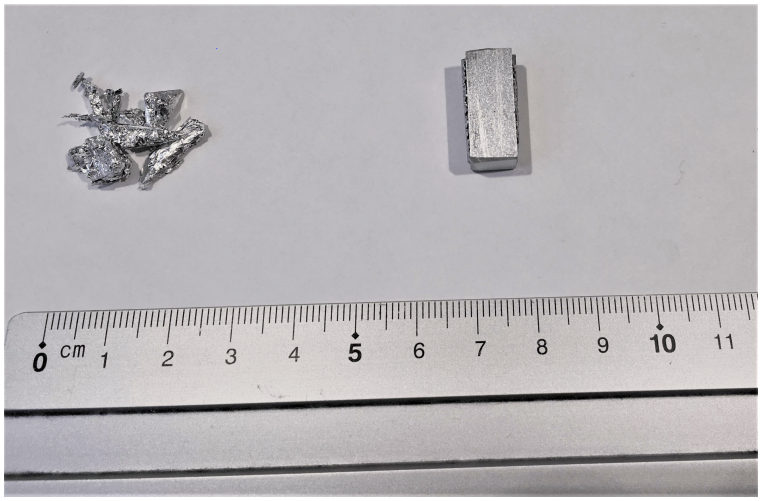

Figure 3.1: Left: granulated aluminium foil. Right: super pure aluminium cubes.

3.1.1 Super pure Aluminium

The material is 4 N (99.99%) pure aluminium, often named Vigeland aluminium (due to the geographic placement of the Norwegian factory that produces the material). It was delivered in round blocks, each weighing about 150g. The chemical composition of the round blocks before cutting can be seen in table 3.1. The blocks were cut into cubes as seen in figure 3.1. The material and chemical composition was provided from Hydro Sunndalsøra.

Table 3.1: Chemical composition for super pure aluminium as-received.

Element	Comp. [Wt%]	Element	Comp. [Wt%]	Element	Comp. [Wt%]
Al	99.9961	Zn	0.00032	Zr	0.00016
Si	0.0005	Ti	0.00095	Co	0.00005
Mg	0.0003	Cr	0.00005	B	0.00015
Cu	0.00027	Ni	0.00037	Ag	0.00019
Mn	0.00006	Pb	0.00014	Sn	0.00033

After screw extrusion another chemical composition test was conducted, from the material plug in front of the screw tip after screw extrusion. The material plug can be seen in step 5 & 6 in figure 3.5. The resulting composition can be seen in table 3.2.

Table 3.2: Chemical composition for super pure aluminium after screw extrusion, for material plug.

Element	Comp. [Wt%]	Element	Comp. [Wt%]	Element	Comp. [Wt%]
Al	99.9807	Ti	0.00119	Zr	0.00018
Si	0.00216	Cr	0.00048	Co	0.00006
Fe	0.01042	Ni	0.00068	P	0.00003
Cu	0.00073	Pb	0.00016	B	0.00021
Mn	0.00078	Sn	0.00035	Ag	0.00019
Mg	0.00078	Na	0.00001		
Zn	0.00041	Ca	0.00047		

3.1.2 Aluminium foil

For the first aluminium foil experiment with a die of 3mm a mix of two different commercial aluminum foils were used. One bought online and the other was purchased from a local retailer. The initial purchase online was not in sufficient for a full screw extrusion, so more had to be bought at a retailer. The chemical composition is from the material plug in front of the screw tip after screw extrusion. The material plug can be seen in step 5 & 6 in figure 3.5. The resulting chemical composition can be seen in table 3.3.

Table 3.3: Chemical composition for aluminium foil with a 3mm die after screw extrusion, for material plug.

Element	Comp. [Wt%]	Element	Comp. [Wt%]	Element	Comp. [Wt%]
Al	98.083	Ti	0.00735	Na	0.00005
Fe	1.23809	Zn	0.00657	Ca	0.00045
Mn	0.4288	Hg	0.00326	Bi	0.00028
Si	0.21026	Ni	0.00263	Co	0.00015
V	0.01465	Sn	0.00146	Be	0.00001
Ga	0.01098	Zr	0.00067	Ag	0.0002
Cu	0.00825	B	0.00084	P	0.00003

For the aluminium foil experiment with a 10mm die, only one type of aluminium foil was used, purchased from a local retailer. The chemical composition is from the material plug in front of the screw tip after screw extrusion and the material plug can be seen in step 5 & 6 in figure 3.5. The resulting chemical composition is presented in table 3.4.

Table 3.4: Chemical composition for aluminium foil with a 10mm diameter after screw extrusion, in front of screw tip.

Element	Comp. [Wt%]	Element	Comp. [Wt%]	Element	Comp. [Wt%]
Al	97.971	Zn	0.00299	Zr	0.0009
Fe	1.52878	Ti	0.01877	Hg	0.00424
Mn	0.31406	Cr	0.00108	Co	0.00023
Si	0.10676	Mg	0.00072	P	0.00088
V	0.01834	Ni	0.00545	Bi	0.00041
Ga	0.01396	Sn	0.00089	Sb	0.00014
Cu	0.00617	Na	0.00005	B	0.00146
Pb	0.00034	Ca	0.00216	Ag	0.0002

3.2 Screw extrusion feedstock

3.2.1 Super pure aluminium

The collected round blocks were cut into rectangular cubes measuring approximately 20mm in length and a 5mm x 5mm cross-section. This was done by Finmekanisk verksted at NTNU. The different steps can be seen in figure 3.2.

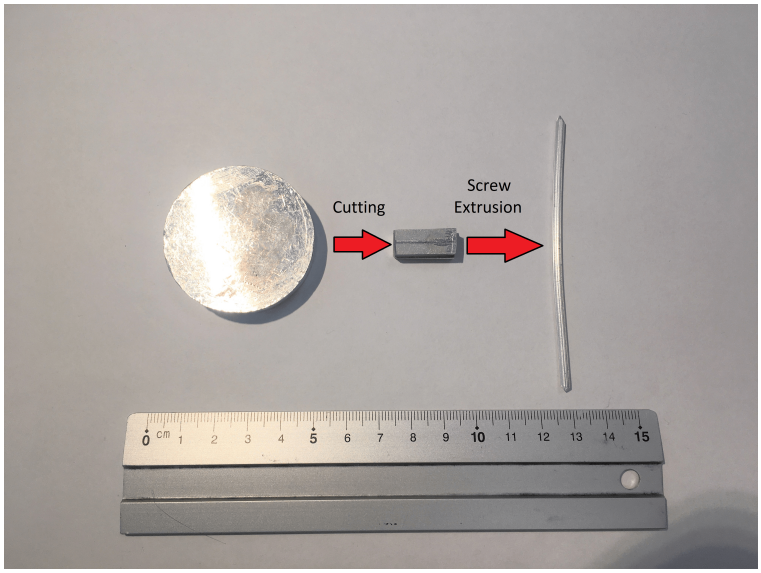

Figure 3.2: Super pure aluminium in different forms throughout this thesis.

3.2.2 Aluminium foil

The aluminium foil was granulated using a Getecha Granulator. The process can be seen in figure 3.3 and starts with compacting the foil into a ball, that is then dropped into the granulator. Metal blades cuts and compacts the aluminium foil into small granules. Some pieces of this can be seen in figure 3.1 in section 3.1.

Figure 3.3: Getecha granulator used to granulate aluminium foil.

The granulated feedstock was screw extruded in two different experiments, one with a 3mm die, and one with a 10mm die. The different forms of aluminium foil throughout this thesis can be seen in figure 3.4.

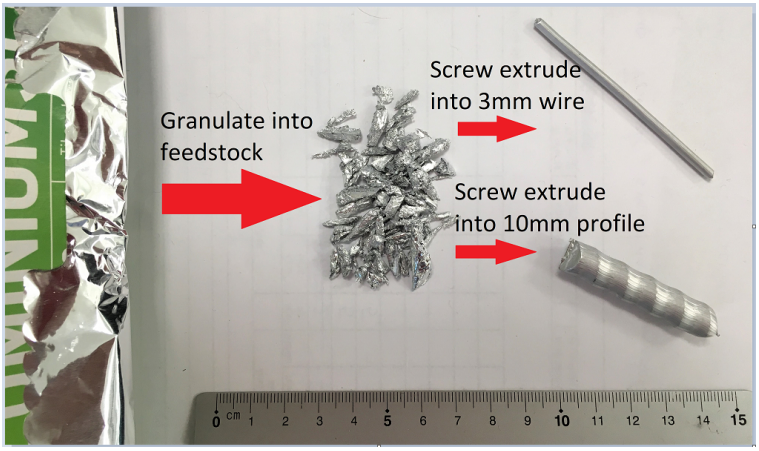

Figure 3.4: Aluminium foil in different forms throughout this thesis.

3.3 Screw extrusion process

A screw extruder prototype was used for the extrusions in this master's thesis. It was located at Institute of Materials Science at NTNU.

3.3.1 Operating procedure

The procedure is summarized in figure 3.5. The die was preheated to approximately 350°C using an induction coil before the experiments started, step 2 in figure 3.5. This was done to decrease the flow stress of the aluminium as it is being extruded. The feedstock described in section 3.1 was poured into the feeding hole gradually using a vibration feeder. The feeding rate is approximately 0,4 grams/second, however the feeding of material is stopped when necessary to avoid overfeeding, see step 3. Compressing the feedstock generates heat, and this was balanced by reducing the induction coil during the experiment and air cooling of the screw extruder (step 4 & 5). After the extrusion was finished, the material plug (seen in step 6) was removed from the screw.

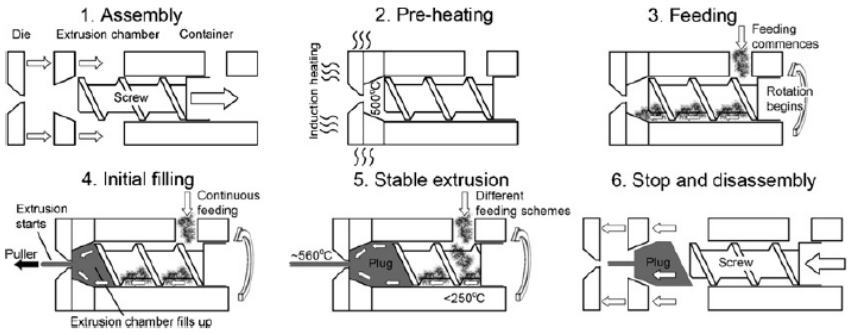

Figure 3.5: Sketch of screw extrusion procedure steps. From[27].

Relevant parameters for the three different screw extrusion experiments run can be seen in table 3.5. The temperature column describes if the operator could maintain a stable temperature ±10°C over a region of at least 30 cm of profile produced. For unstable experiments the temperature increased continuously throughout the experiment from start to finish.

Table 3.5: Screw extrusion experiment abbreviations, notes and parameters

Experiment number	Feedstock material	Extrusion (die) temperature [C]	Die diameter	notes	Name (abbreviation)
1	Super pure aluminium	220	3 mm	~1m extruded unstable temperature	**SP-Al-220**
1	Super pure aluminium	320	3mm	~1m extruded unstable temperature	**SP-Al-320**
2	Aluminium foil mix	450	3mm	~1m extruded unstable temperature	**AlF3-450**
2	Aluminium foil mix	500	3mm	~1m extruded unstable temperature	**AlF3-500**
3	Aluminium foil	450	10mm	~1m extruded stable temperature	**AlF10-450**
3	Aluminium foil	490	10mm	~1m extruded stable temperature	**AlF10-490**

3.3.2 Screw extruded wires

The finished extruded wires had a diameter of 2,80mm to 2,95mm diameter for each of the base materials. The aluminium foil was also extruded using a 10mm die, and had a diameter of 9,50mm to 9,90mm. The surface of the wires changed depending on the temperature and the type of screw used.

3.3.3 Screw geometries

Two different screw geometries were used for screw extrusion in this thesis. A single flight screw and a double flight screw. The geometry of the selected screw for each experiment was chosen based on extruded profile quality versus ease of extrusion process and can be seen in table 3.6. A sketch of the screw geometries can be seen in figure 3.6.

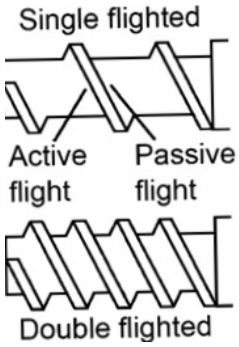

Figure 3.6: Sketch of screw geometries. From[27]

The first two experiments were conducted with a 3mm die opening, while the last experiment (aluminium foil experiment number two) were conducted using a 10mm die opening. Both dies gave a round profile.

Table 3.6: Screw geometry chosen for each experiment

Experiment	Screw geometry [thickness]
3mm super pure aluminium wire	Double [80mm]
3mm aluminium foil wire	Double [80mm]
10mm aluminium foil profile	Single [80mm]

3.4 Electrical conductivity measurements

The 3mm wires were tested in an AOIP OM21 microhmmeter. The wires were cleaned in ethanol and dried at 120°C for at least one hour to remove moisture before testing. Two of the wires tested can be seen in figure 3.7.

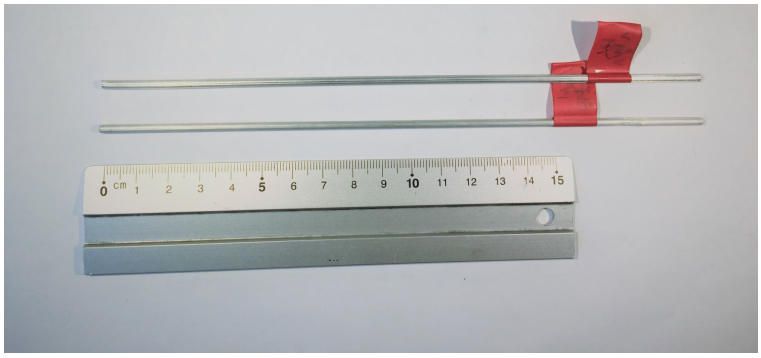

Figure 3.7: Picture of screw extruded wires to be electrical resistivity tested. Red tape is used for identification of sample.

As seen in figure 3.8 the wires were clamped down with two blue clamps onto an electrically conducting plate. The voltage was measured using two contact points that were 98.45mm apart. Figure 3.8 shows the OM21 apparatus. The pulse current setting was used with 20mV sent through the specimens. For even more accurate measurements the DC current setting should be used, however this setting is broken in the apparatus. The resistance given is in temperature independent mode, with a temperature varying between 22-24°C entered into the OM21. This was measured using a K-type thermocouple. For the area measurements, the diameter was measured at six points along the length of the electrical wire using a caliper. The resistances given by the apparatus was converted to electrical conductivity by the equations given in section 2.3.2. The density was calculated based on the theoretical densities of each alloying element times its fraction in the alloy.

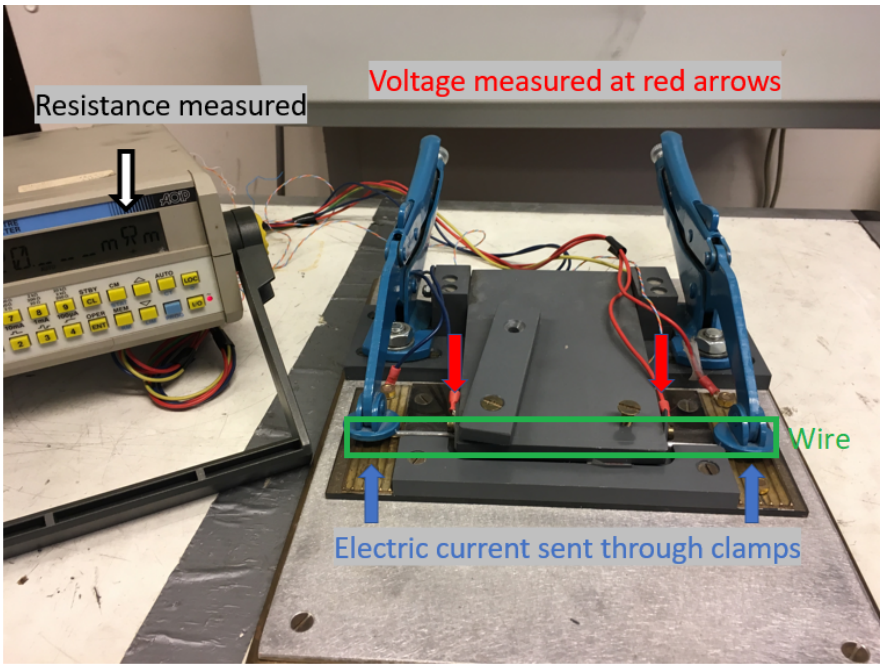

Figure 3.8: Picture of electrical resistance measurement by OM21 apparatus.

3.5 Hardness testing

Before hardness testing 10mm lengths of the wires were cut out. These were then moulded in Clarocit epoxy. The cross-section was grinded with P500 & P1200 sandpaper using an ATM Saphir 330. The hardness, given in HV was measured using a Zwick/Roell ZHV 30 hardness tester with a load of 1Kg. Each sample was tested five times at different places on the sample cross-sectional surface.

3.6 Tensile testing

The screw extruded products were tested by uniaxial tensile testing to identify mechanical properties. The 10mm diameter screw extruded Aluminium foil was machined into cylindrical tensile rods at Finmekanisk Verksted. The specification can be seen in figure 3.9.

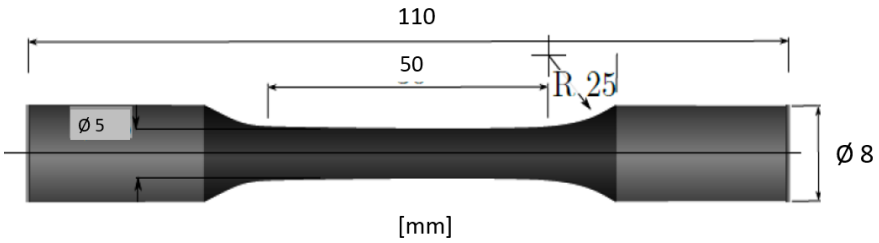

Figure 3.9: Sketch of tensile rods for tensile testing of 10mm screw extruded aluminium foil with dimensions. Modified from[28]

The 10mm samples were tested in a MTS 810 material testing system, and three specimens can be seen in figure 3.10, where one is fractured. The crosshead speed was 2mm/minute with a 25mm extensometer for the MTS 810.

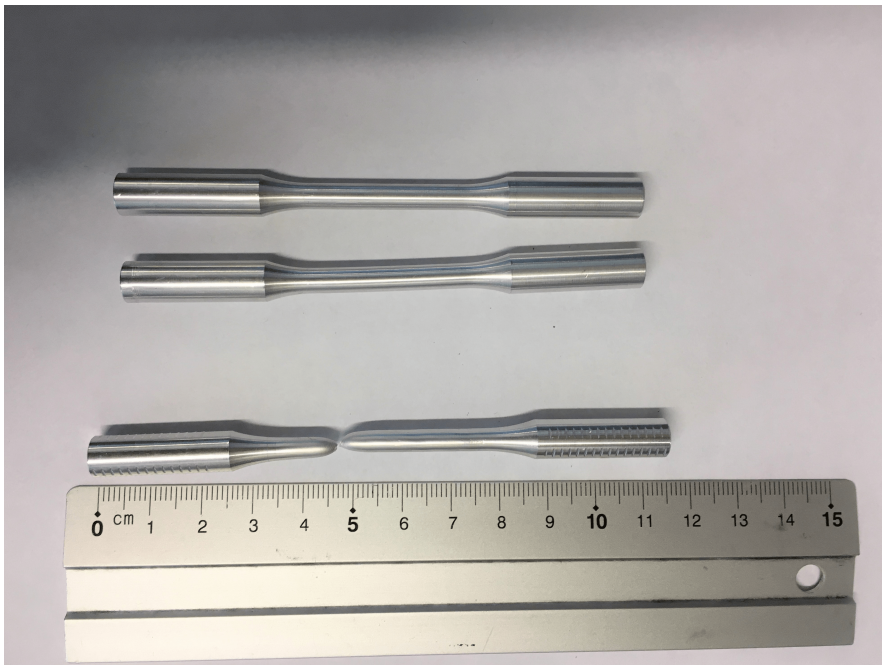

Figure 3.10: Picture of tensile rods for tensile testing of 10mm screw extruded aluminium foil.

The screw extruded 3mm wires were tested using a Zwick Roell 2.5kN tensile test machine. As these samples were too narrow to be machined into tensile rods, copper clamps were attached to the ends to ensure no sliding occurred. Figure 3.11 shows 3mm wire without clamps(top), with clamps(middle) and clamped clamps(bottom). The copper clamps were attached to the wires using a Proskit 6PK-301H. The first tensile tests were clamped too hard, causing the fracture to occur at the grips. The last tensile tests were successful, however lack of material limited the number of tensile tests that could be run. As the wires were not straight, a pre-set force of 100N was set before the tensile test was initiated.

Figure 3.11: Picture of tensile wires for tensile testing of 3mm screw extruded aluminium.

3.7 Metallographic imaging

15mm lengths of the wires were cut out and moulded in Epofix epoxy. The SiC grinding was accomplished using a Struers Rotopol-31, and the polishing was conducted using a Struers Tegrapol-31. Finally, the samples were vibration polished for 6 hours using a Buehler Vibromet 2. Single samples mode was used with a force of 10N for each sample due to the low strength of pure aluminium. The different steps are detailed in table 3.7. An annealing time of 60 seconds were enough to display the grain boundaries for light optical images.

Table 3.7: Polishing steps for optical microscopy and SEM imaging

Process	Roughness	Machine	Velocity	Cleaning
Grinding	#FEPA 320	Struers Rotopol 31	150	Water + soap
Grinding	#FEPA 500	Struers Rotopol 31	150	Water + soap
Grinding	#FEPA 800	Struers Rotopol 31	150	Water + soap
Grinding	#FEPA 1200	Struers Rotopol 31	150	Water + soap
Polishing	Diapro Largo 9	Struers Tegrapol 31	150	Water + soap, Ethanol + drying
Polishing	Diapro Mol 3	Struers Tegrapol 31	150	Water + soap, Ethanol + drying
Polishing	Diapro Nap B1	Struers Tegrapol 31	150	Water + soap, Ethanol + drying
Polishing	Mastermet 2	Buehler Vibromet 2	150	Water + soap, Ethanol + drying

3.8 Annealing of screw extruded 3mm wires

To assess the effects of heat treatment on screw extruded wires the 3mm screw extruded wires were annealed in a Nabertherm N15 furnace. The screw extruded super pure aluminium and the 3mm screw extruded aluminium foil were annealed at 200°C and 500°C for 30 minutes. After annealing the wires were re-tested and their microstructure imaged to classify the effect.

3.9 Density measurements

The density of the aluminium foil samples were tested using an Accupyc II 1340. The Accupyc was used with helium gas with the sample contained in a 10cc container. For each extrusion, material from all sections were combined to one density measurement to acquire enough material. This means that the effect of extrusion temperature cannot be assessed. One measurement was performed for screw extruded super pure aluminium, one for screw extruded aluminium foil with a 3mm die, and another one for 10mm die.

The contrast mapping was done using the iDT software with help from Senior Engineer Trygve Schanche. Both optical microscopy and scanning electron microscopy images were used.

4 Results

4.1 Screw extruded super pure aluminium 3mm wire

4.1.1 Electrical conductivity

As screw extruded

The electrical conductivity of screw extruded super pure aluminium 3mm wire, is presented in figure 4.1. At the end, a reference wire named "referanse A, Vigeland aluminium" is added. This wire is used to calibrate the apparatus. The reason for only two parallels is due to insufficient amount of material extruded. The result show that the conductivities based on equation 2.4(density) gives very similar results, while the conductivities based on equation 2.3(area) are much more varying. The reference wire has a similar conductivity as the screw extruded wires if the calculations are based on equation 2.4(density).

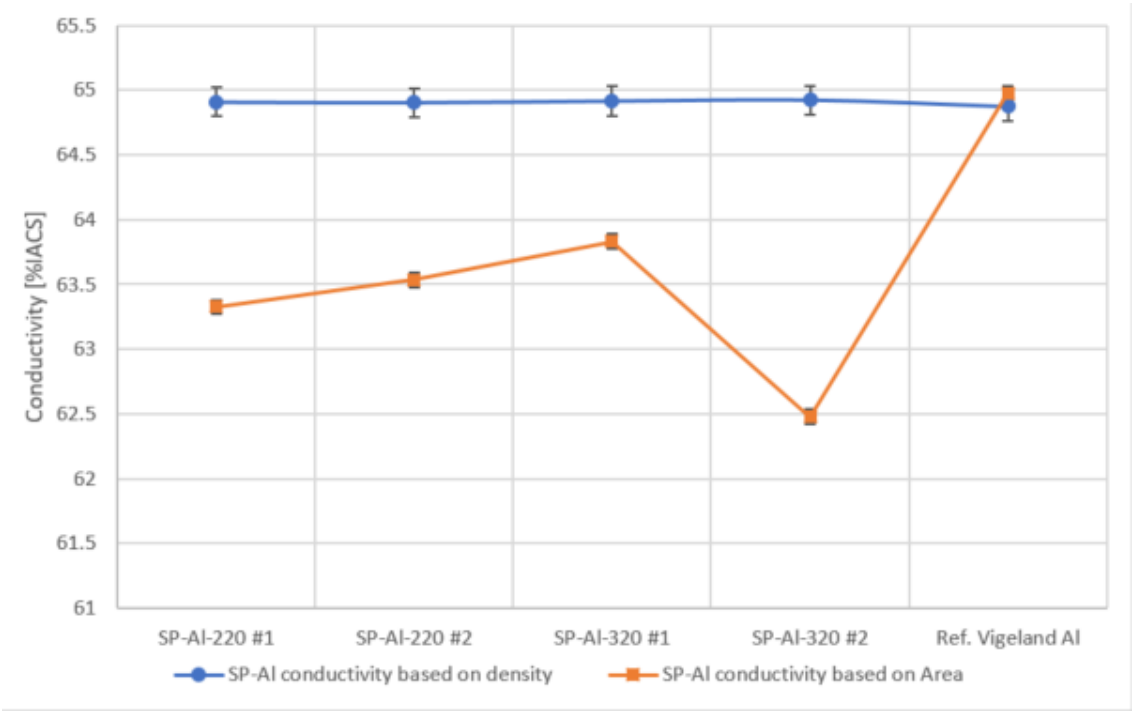

Figure 4.1: Electrical conductivity for SP-AL, with a reference 3,47mm wire labelled Vigeland aluminium.

After annealing

The electrical conductivity after annealing at 150°C and after annealing at 500°C is shown in figure 4.2. Only the conductivities based on equation 2.4 are presented due to more stable results. The results show a decrease in conductivity after annealing the screw extruded wires for both temperatures compared to the screw extruded sample as-is. The conductivity is very slightly increased by annealing at 500°C compared to 150°C.

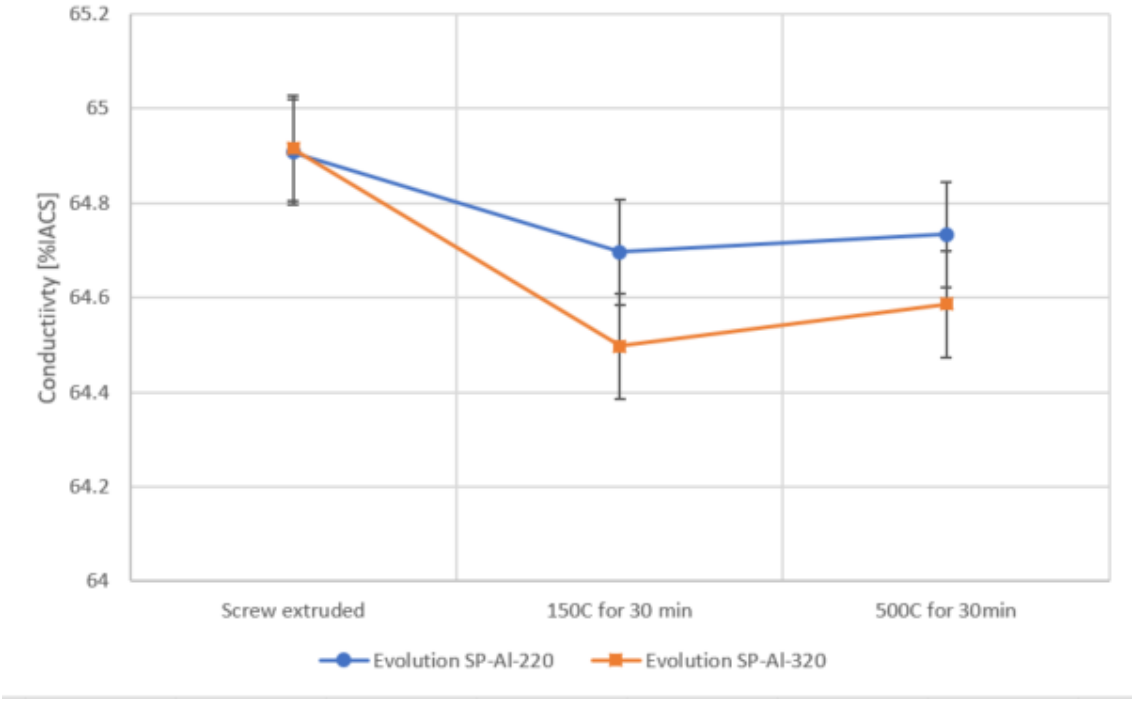

Figure 4.2: Electrical conductivity evolution for SP-Al from no annealing (left) to 150°C annealing for 30 minutes (middle) to 500°C annealing for 30 minutes (right).

4.1.2 Hardness

The change in hardness for super pure aluminium wire after different processing steps, is presented in figure 4.3. The hardness is measured in Vickers hardness. There were different screw extruded samples used for each heat treatment, so the 500°C annealed sample was not annealed at 150°C prior. The results show that the hardness increases significantly from the feedstock to screw extruded state. The hardness increases slightly after annealing at 150°C for 30 minutes, but decreases sharply when annealed at 500°C for 30 minutes.

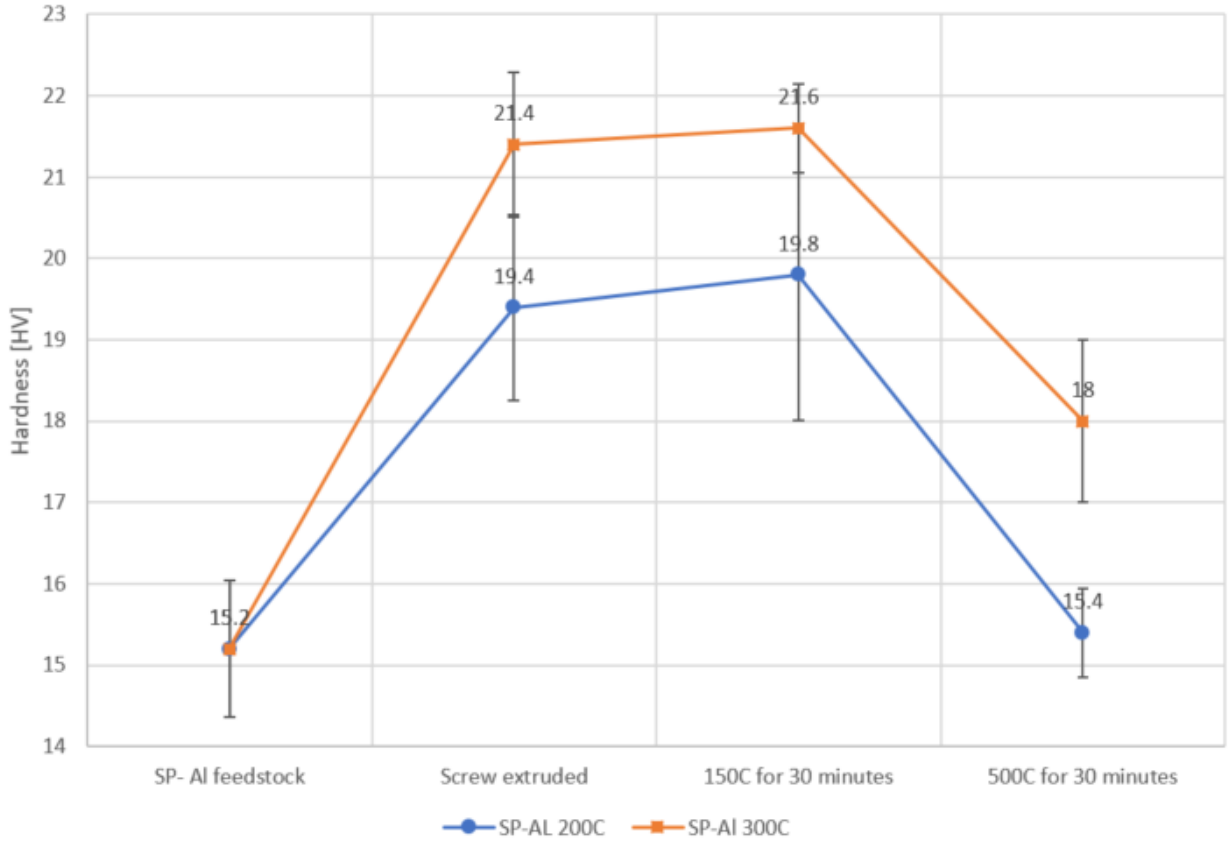

Figure 4.3: Hardness evolution from feedstock to screw extruded to two different heat treatments. The heat treatments are 150°C annealing for 30 minutes and 500°C annealing for 30 minutes.

4.1.3 Tensile strength

The tensile tests done on screw extruded super pure aluminium 3mm wire is presented in figure 4.4. As there were not much material left for these tests, they were all taken from the middle section of the wire, with an extrusion(die) temperature of 270°C ±10°C. The tests show a stable yield strength of 35 MPa and a stable ultimate tensile strength of 43 MPa. The strain at fracture varies for all samples. The sample with the lowest strain shows a faster work hardening prior to necking, and the sample with the highest strain shows a slower work hardening prior to necking.

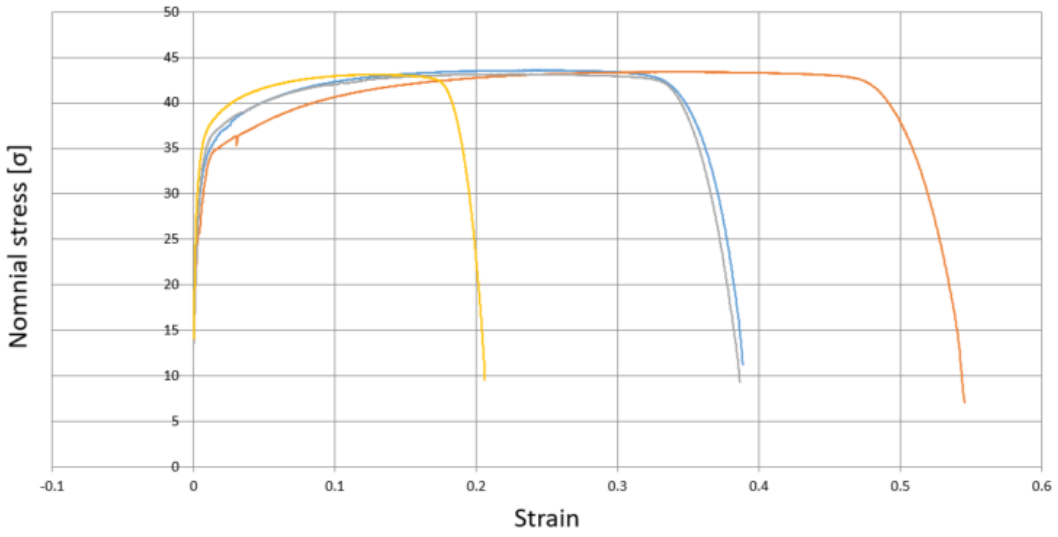

Figure 4.4: Tensile tests for SP-Al. Due to low amount of material all specimens are taken from an extrusion(die) temperature of about 270°C. The tests are parallels.

4.1.4 Light optical microscopy

As screw extruded

The resulting microstructure of anodized screw extruded 220°C super pure 3mm wire is presented in figure 4.5. The magnification is 25X. The cross-sectional image (a) shows some cracking in a circular pattern. There is some abnormal grain growth in the lower part of (a), and in the middle of (b).

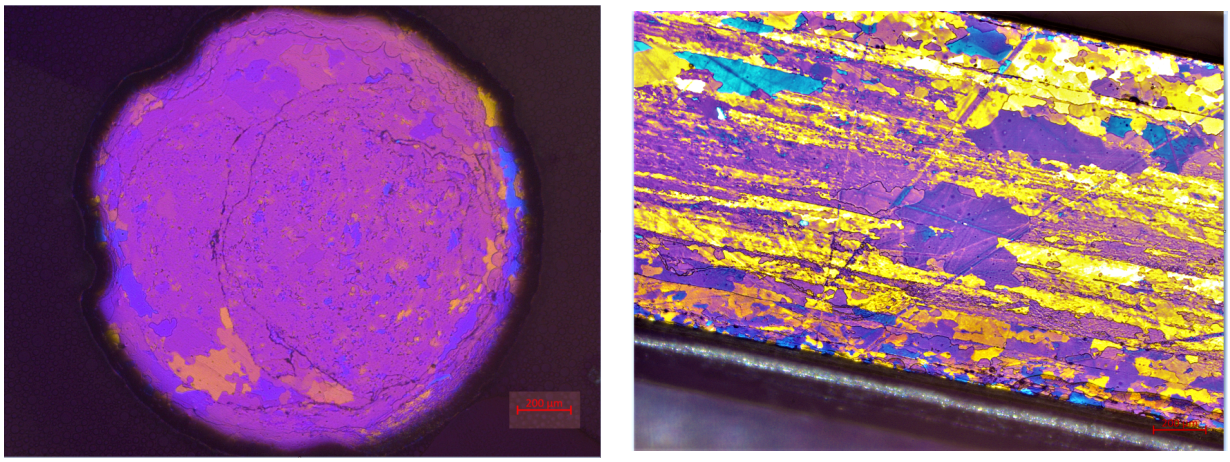

(a) (b)

Figure 4.5: (a) Cross sectional image of anodized SP-Al-220. (b) Longitudinal image of anodized SP-Al-220.

The resulting microstructure of anodized screw extruded 320°C super pure aluminium 3mm wires is presented in figure 4.6. The magnification is 25X. The microstructure shows equiaxed grains in the outer edges with a deformed structure in the middle. (b) shows abnormal grain growth in the middle, with slightly elongated grains. There are also some horizontal dark stripes in (b).

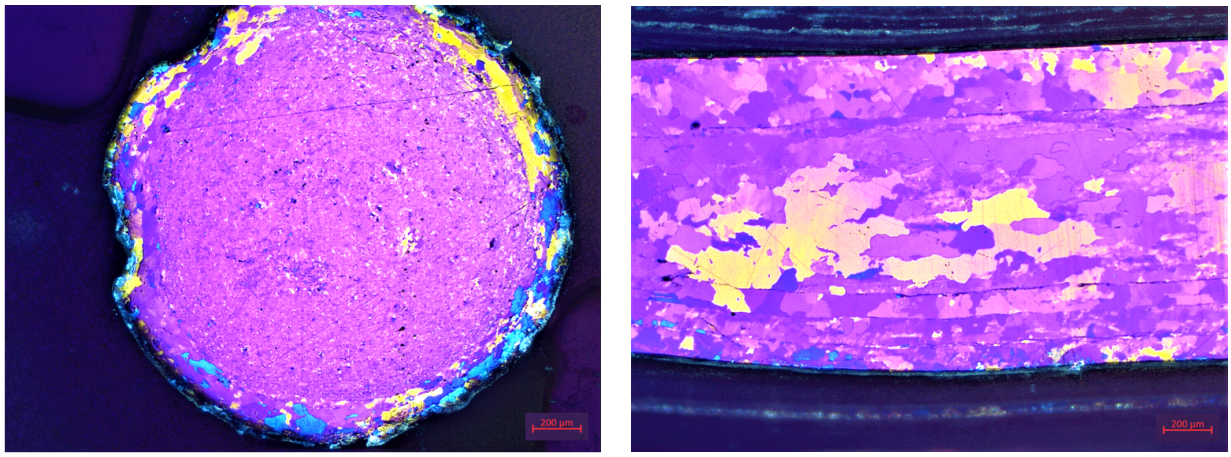

(a) (b)

Figure 4.6: (a) Cross sectional image of anodized SP-Al-320. (b) Longitudinal image of anodized SP-Al-320.

After annealing

The resulting microstructure of anodized screw extruded 220°C super pure aluminium 3mm wire after annealing is presented in figure 4.7. The magnification is 25X. The change in microstructure after annealing at 150°C is not very significant, however after annealing at 500°C the effect is significant. The material is completely recrystallized, and in the bulk very large grains have grown.

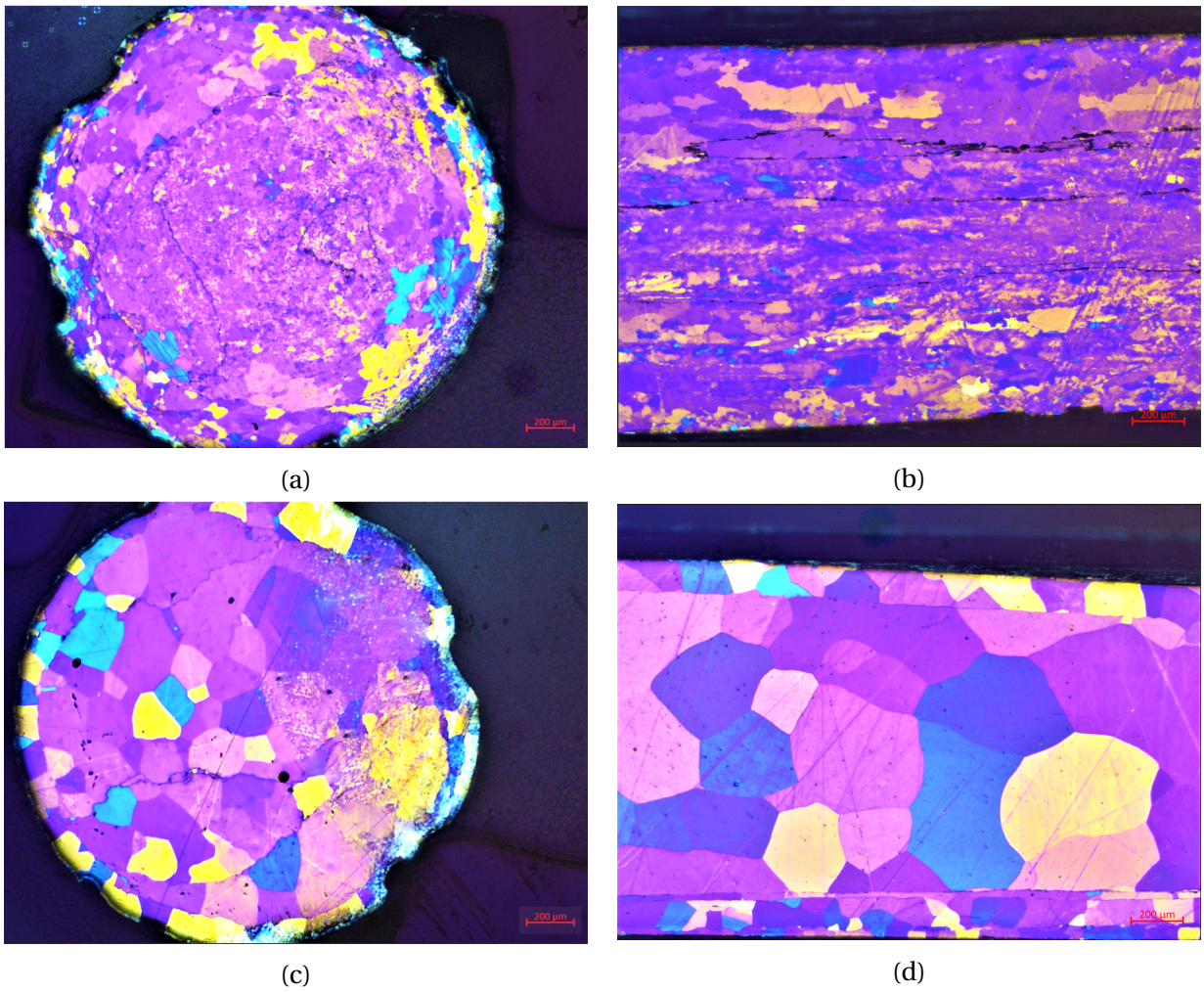

(a) (b)

(c) (d)

Figure 4.7: (a) Cross-sectional image of anodized SP-Al-220 annealed at 150C for 30 minutes. (b) Longitudinal image of anodized SP-Al-220 annealed at 150C for 30 minutes. (c) Cross-sectional image of anodized SP-Al-220 annealed at 500C for 30 minutes. (d) Longitudinal image of anodized SP-Al-220 annealed at 500C for 30 minutes.

The resulting microstructure of anodized screw extruded 320°C super pure aluminium 3mm wire after annealing is presented in figure 4.8. The magnification is 25X. Here the material is recrystallized after annealing at 150°C. Annealing at 500°C (picture (c)) does not show significant grain growth.

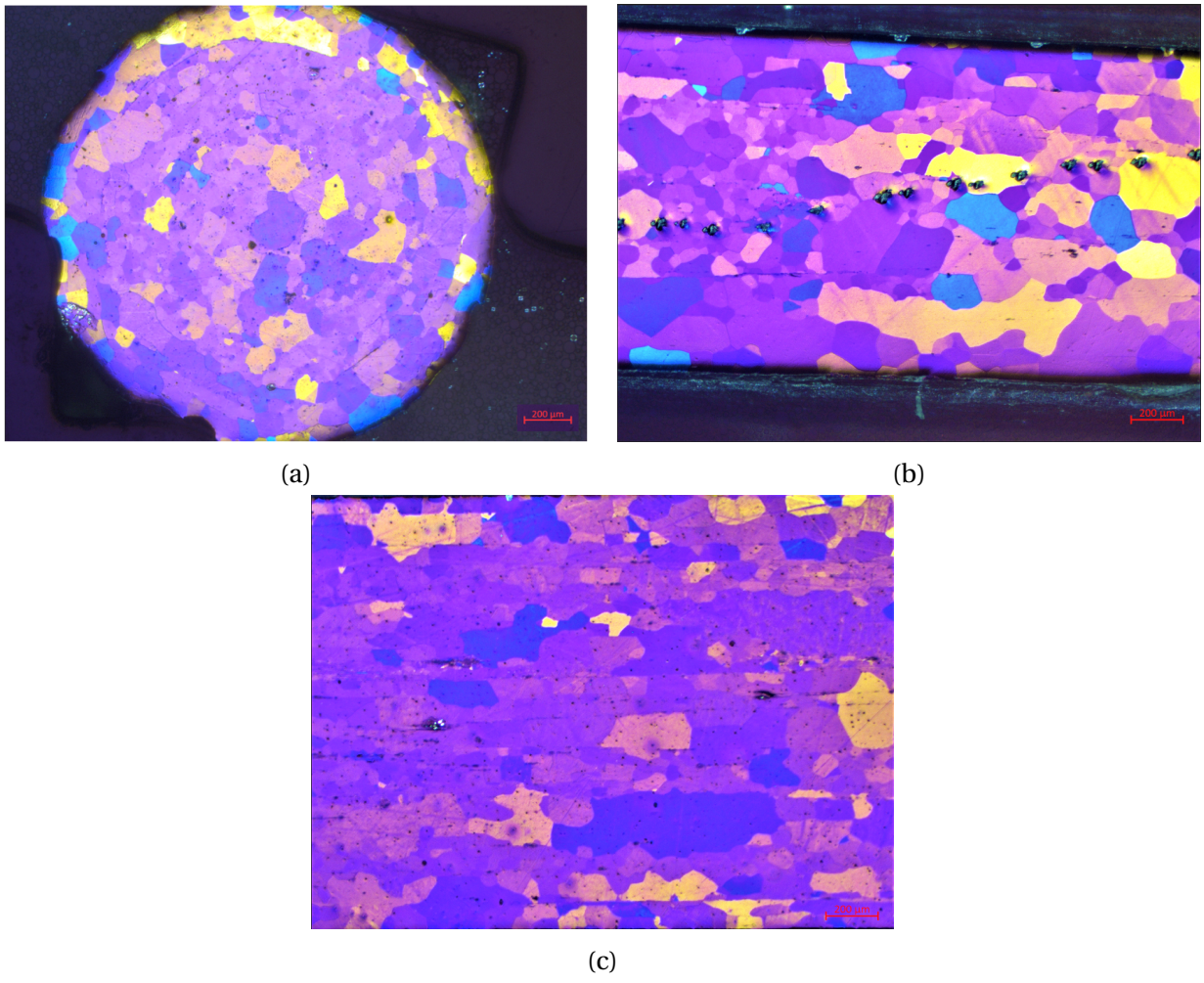

(a) (b)

(c)

Figure 4.8: (a) Cross sectional image of anodized SP-Al-320 annealed at 150C for 30 minutes. (b) Longitudinal image of anodized SP-Al-320 annealed at 150°C for 30 minutes. (c) Longitudinal image of anodized SP-Al-320 annealed at 500°C for 30 minutes.

4.1.5 Scanning Electron Microscopy (SEM)

A polished sample of super pure 320°C aluminium wire was imaged by SEM to determine if there are any particles on the surface and if so, the type of the particles and their distribution. Figure 4.9 shows the surface at 100X magnification, but no particles are seen. There are black spots seen on the polished surface indicating gas pores.

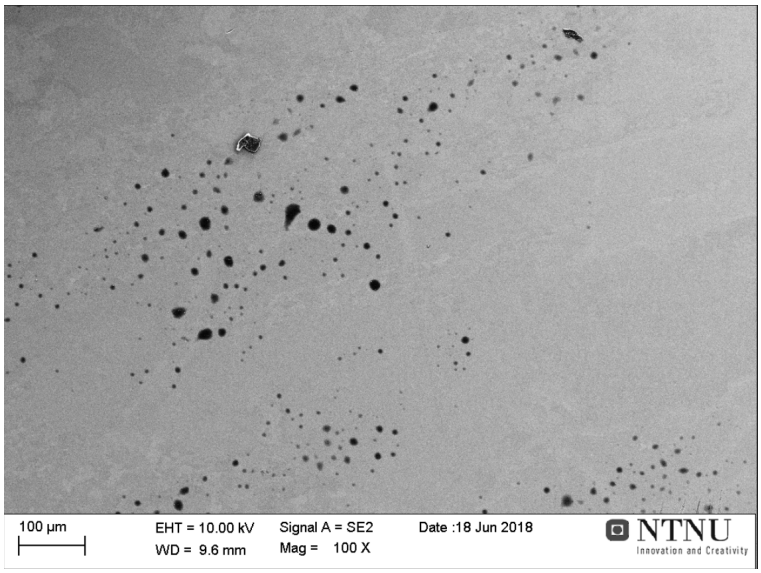

Figure 4.9: circular holes on surface of SP-Al-320, 100X magnification.

4.1.6 Density

The density as measured by pycnometer and contrast area mapping is described in table 4.1. The contrast area mapping is done using iSolution DT software on figure 4.9. The results show that the density is over 99% measured by pycnometer, and just over 98% measured by Image contrast with a SEM picture.

Table 4.1: Density of SP-Al using different techniques. SEM = Scanning electron microscope.

Method	Density [g/cm^3]	Percent of theoretical
Theoretical density	2,6995	100%
Pycnometer	2,6746	99.1%
SEM contrast	2.6536	98.3%

4.2 Screw extruded aluminium foil based 3mm wire

4.2.1 Electrical conductivity

As screw extruded

The electrical conductivity of screw extruded aluminium foil based 3mm wire, is presented in figure 4.10. The reason for using only two parallels is due to insufficient amount of material extruded. The conductivities vary substantially between each parallel, and based on how the conductivities are calculated. They also vary substantially according to how the conductivity is calculated.

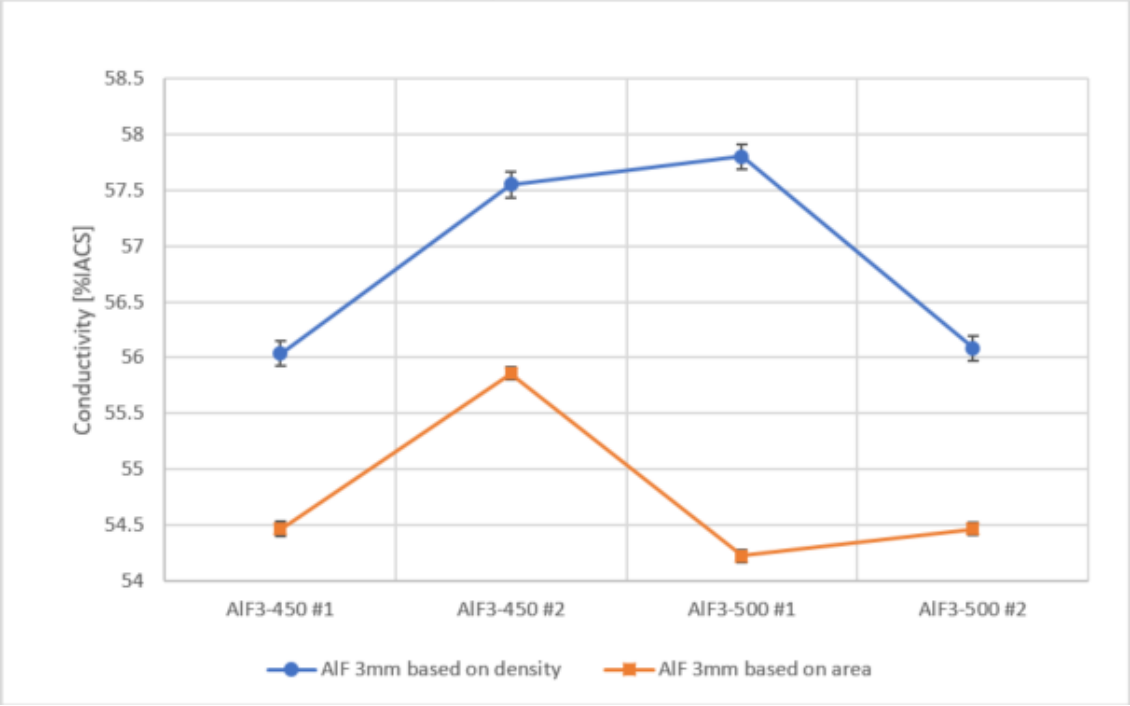

Figure 4.10: Electrical conductivity for AlF3 wires.

After annealing

The electrical conductivity after annealing at 150°C and after annealing at 500°C is shown in figure 4.11. Only the conductivities based on equation 2.4 are presented. The change in electrical conductivity is small for annealing at 150°C, showing a dip for AlF3-450 that is outside the standard deviation for the non-annealed state. For the AlF3-500 the conductivity drops sharply after annealing at 500°C, while the change is slightly positive for AlF3-450.

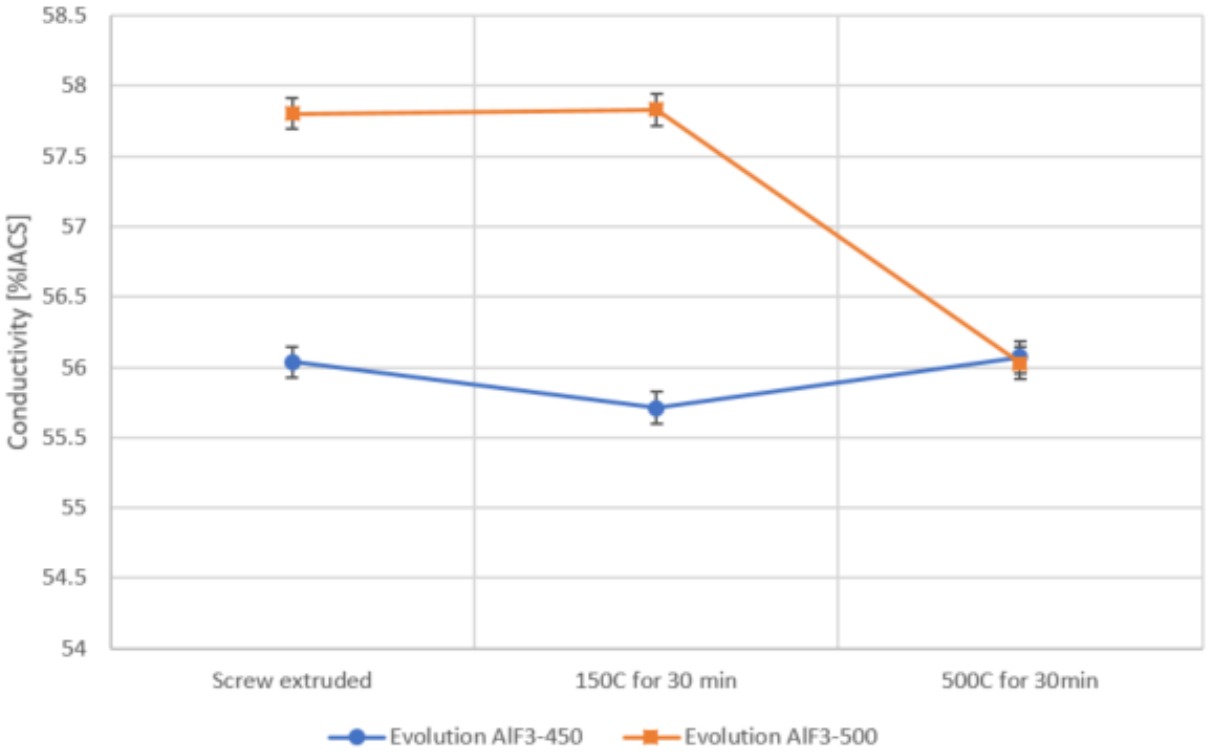

Figure 4.11: Evolution of electrical conductivity for AlF3 wires after different annealing steps.

4.2.2 Calculated conductivity based on chemical composition

The electrical conductivity was calculated based on the contributions of foreign elements as seen in figure 2.9 based on the chemical analysis presented in table 3.3.

The result shows a calculated conductivity of 57,18% IACS. Due to the high amount of Fe (1.24%) the curve for Fe in figure 2.9 was extrapolated linearly. Some trace elements were not present in

the figure, and was not accounted for. Nickel, mercury and tin all account for less than 0.01% of the alloying content, so their effect should be minimal.

4.2.3 Hardness

The change in hardness for screw extruded aluminium foil based 3mm wire after different processing steps, is presented in figure 4.12. The hardness is measured in Vickers hardness. There were different screw extruded samples used for each heat treatment, so the 500°C annealed sample was not annealed at 150°C prior. The results show that the hardness is increased after annealing at 150°C for both samples, with a decrease after annealing at 500°C.

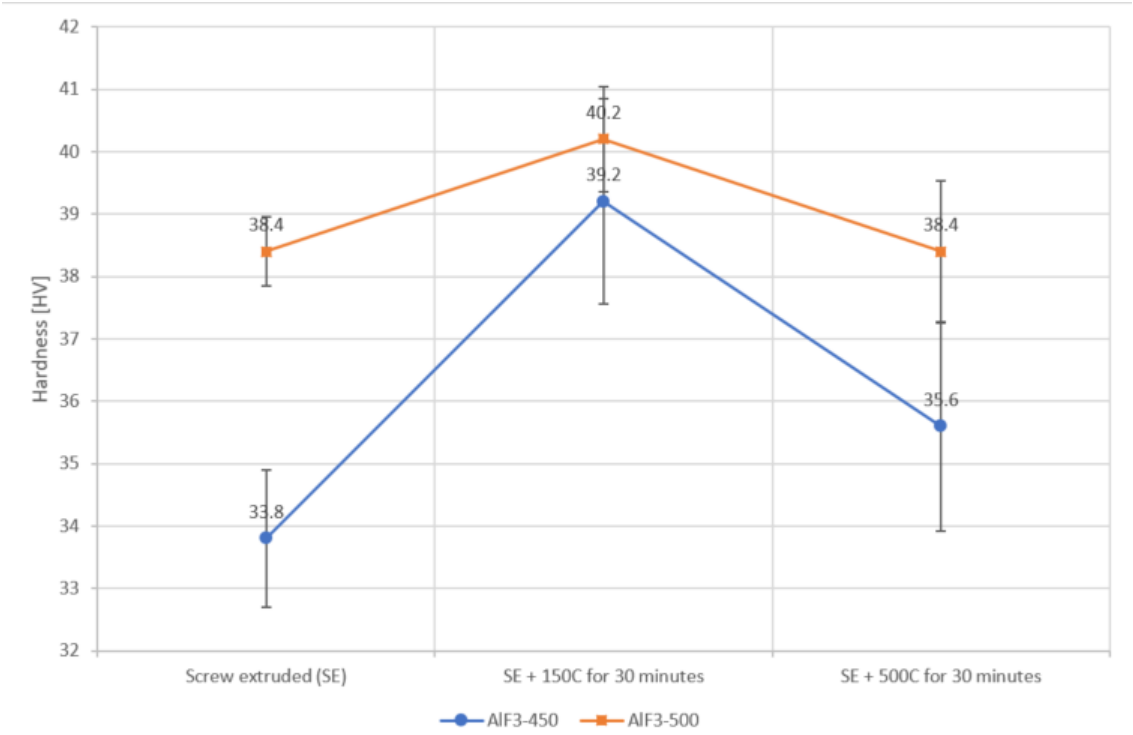

Figure 4.12: Hardness evolution from screw extruded state to two different heat treatments. The heat treatments are 150°C annealing for 30 minutes and 500°C annealing for 30 minutes.

4.2.4 Tensile strength

The tensile tests done on screw extruded 3mm aluminium foil wire is presented in figure 4.13. As there were not much material left for these tests, they were all taken from the middle section of the wire, with an extrusion(die) temperature of 475°C ±10°C. The tests show a stable yield strength of 70 MPa and a stable ultimate tensile strength of 110 MPa. The fracture-strain is the same for both normal samples at about 55% elongation.

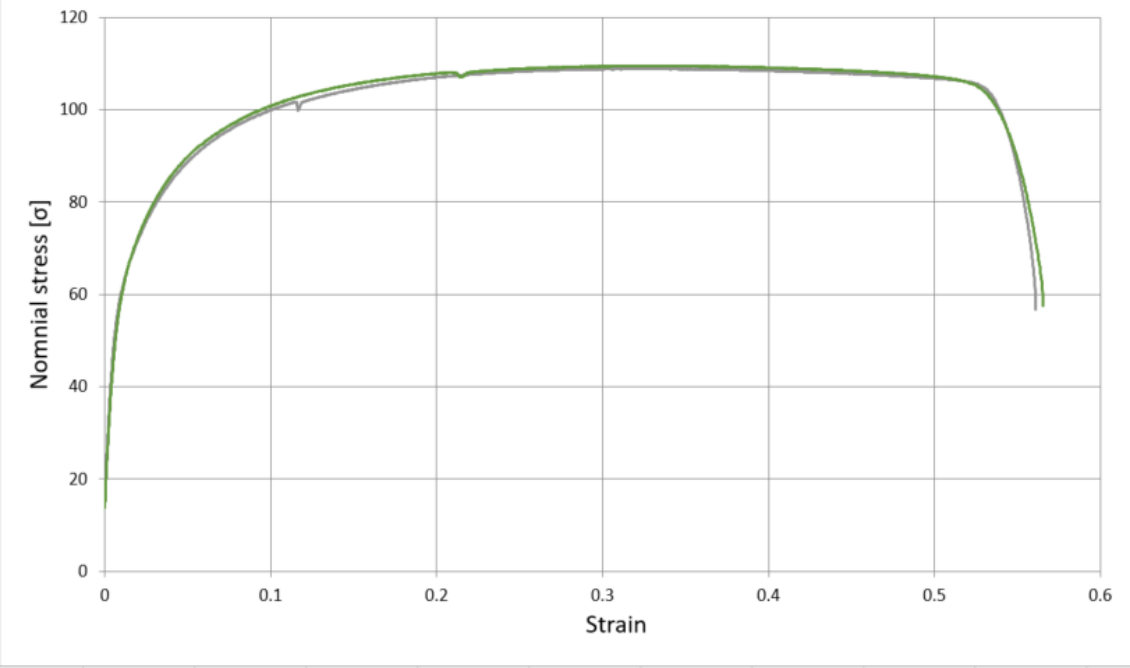

Figure 4.13: Tensile tests for AlF3 wire. Due to low amount of material both specimens are taken from an extrusion(die) temperature of about 475°C. The tests are parallels.

4.2.5 Fractography

One of the successfully tensile tested screw extruded aluminium foil based 3mm wire samples was investigated in SEM to determine the fracture type. Figure 4.14 shows the fracture surface. The images show mainly dimple formation with some impurities (20μm) at the fracture surface, with a shiny colour. The red square in (a) indicates where the picture (b) is taken. Picture (b) shows mainly dimple formation, with a large particle/impurity. From picture (a) the surface shows a circular pattern with uneven topology.

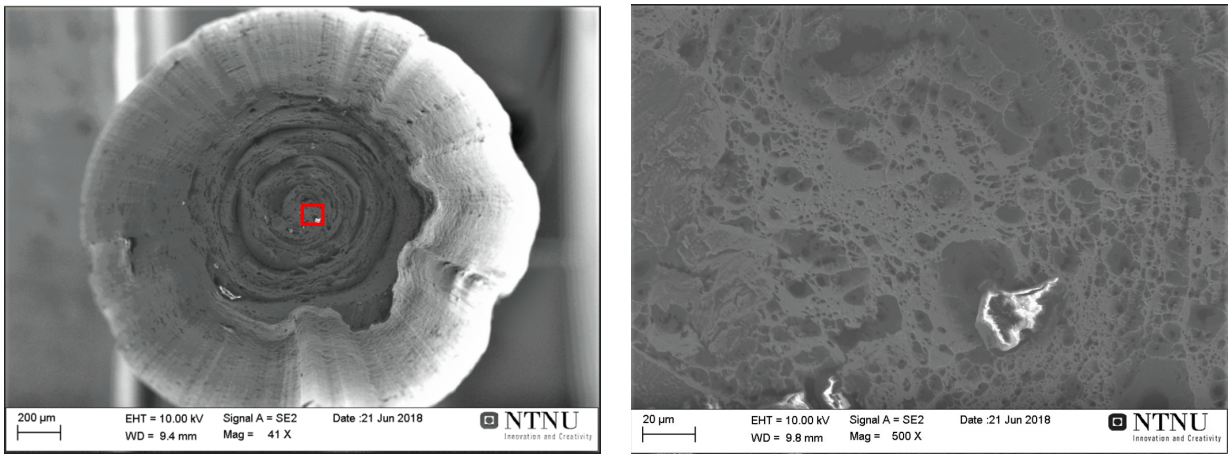

(a) (b)

Figure 4.14: (a) Macroscopic SEM-image of fracture surface for tensile tested AlF3. (b) SEM-image of fracture centre at 200X magnification showing a large particle.

4.2.6 Light optical microscopy

As screw extruded

The resulting microstructure of anodized screw extruded aluminium foil based 450°C 3mm wire is presented in figure 4.15. The magnification is 25X for (a) and (c), with 200X magnification for b) and d). Due to long anodizing times for (c) and (d) and high iron content, some corrosion occurred during anodizing, causing black spots on the 25X magnification images. The images show a very fine-grained structure with a fibrous structure as seen in (c) and (d).

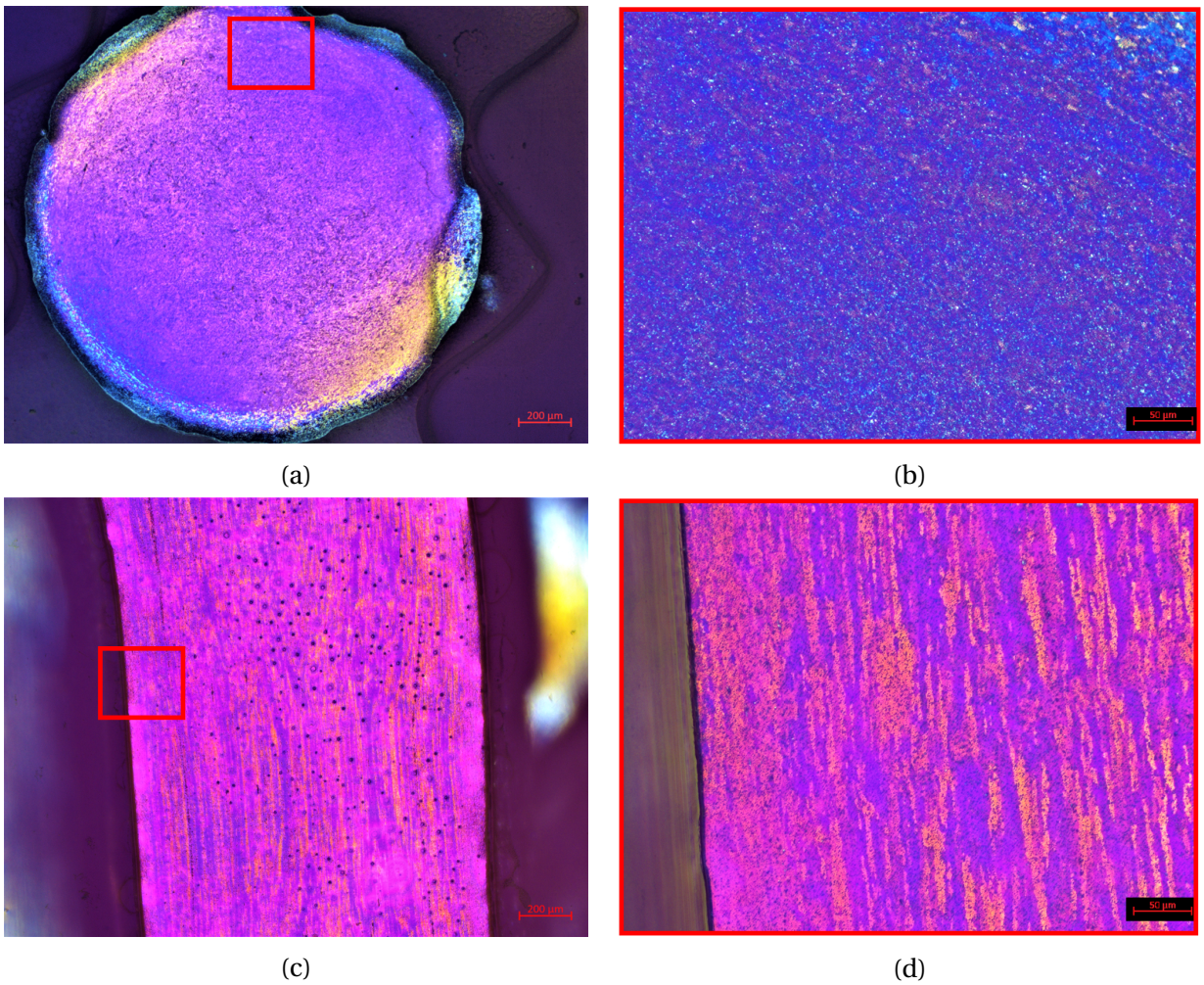

(a) (b)

(c) (d)

Figure 4.15: (a) Cross-sectional image of anodized AlF3-450 at 25X magnification. (b) Cross-sectional image of anodized AlF3-450 at 200X magnification. (c) Longitudinal image of anodized AlF3-450 at 25X magnification. (d) Longitudinal image of anodized AlF3-450 at 200X magnification.

The resulting microstructure of anodized screw extruded aluminium foil based 500°C 3mm wire is presented in figure 4.16. The magnification is 25X for (a) and (c), with 200X magnification for (b) and (d). Here we see the same trends as Alf 3mm 450°C with a fibrous structure and very small grains. (b) shows a circular pattern with particles originating in the centre.

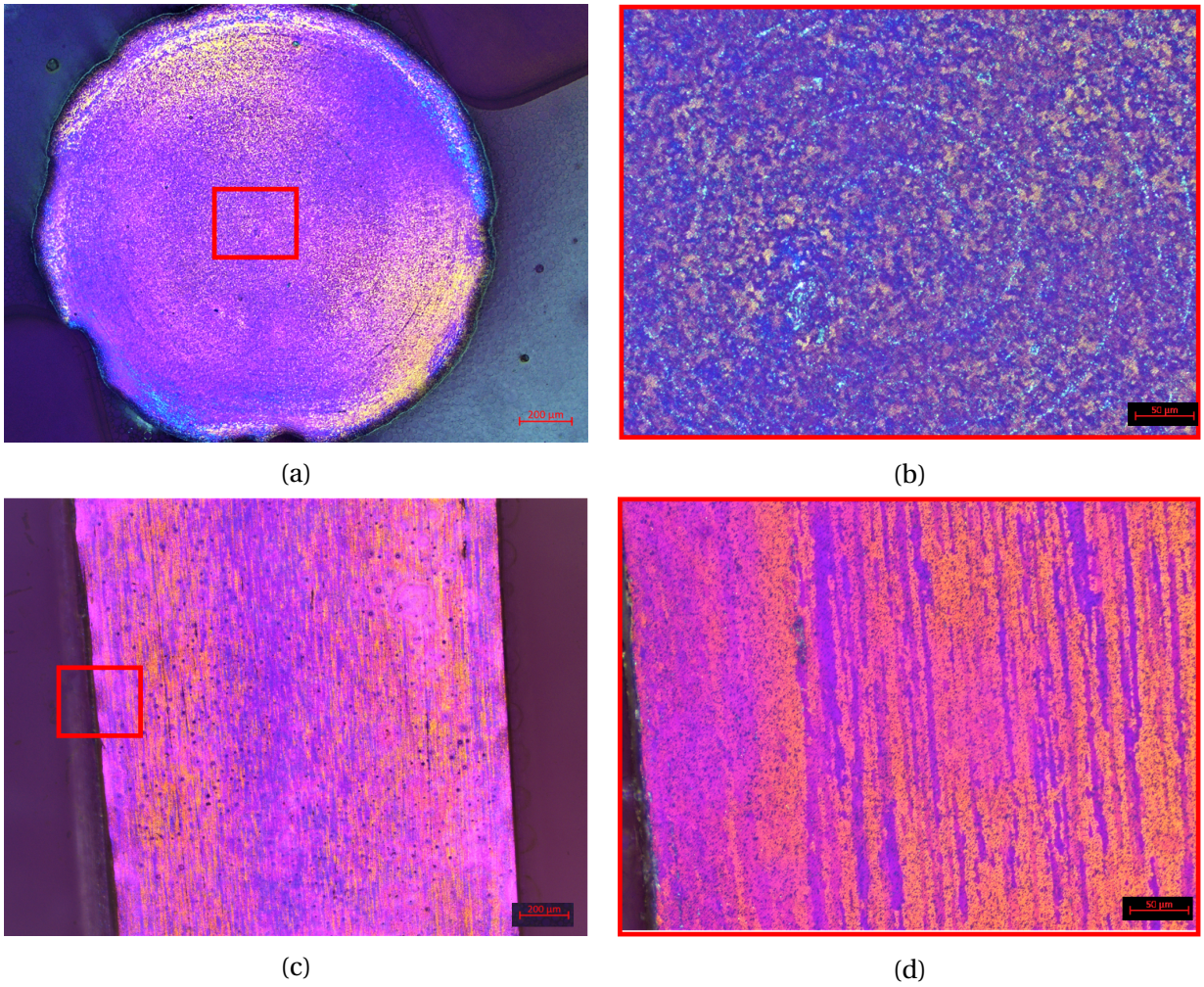

(a) (b)

(c) (d)

Figure 4.16: (a) Cross-sectional image of anodized AlF3-500 at 25X magnification. (b) Cross-sectional image of anodized AlF3-500 at 200X magnification. (c) Longitudinal image of anodized AlF3-500 at 25X magnification. (d) Longitudinal image of anodized AlF3-500 at 200X magnification.

After annealing

The resulting microstructure of anodized screw extruded aluminium foil based 450°C 3mm wire after annealing is presented in figure 4.17. The magnification is 25X for (a) and (c), with 200X magnification for b) and d). The change after annealing is minimal for all images, and no clear trends can be seen.

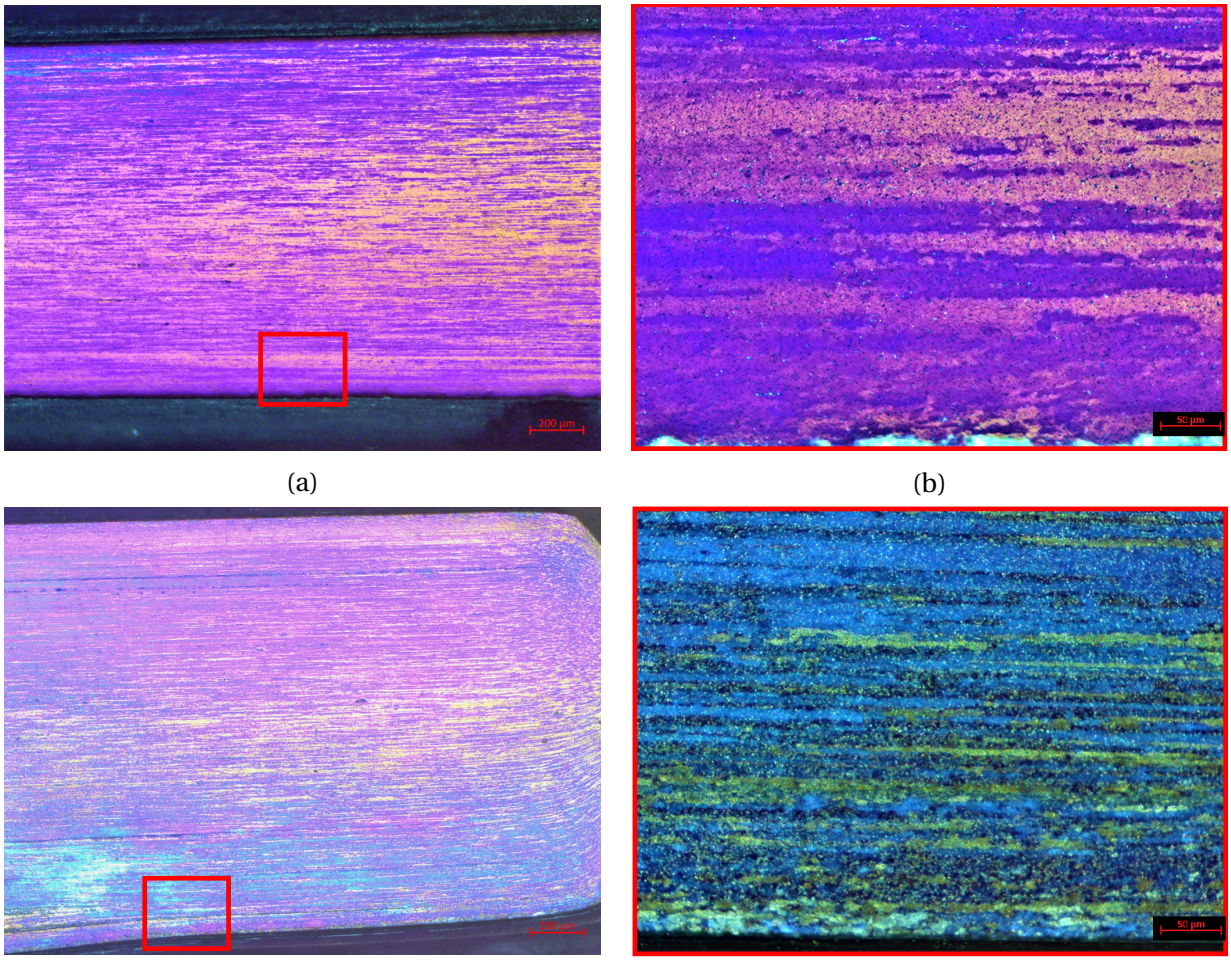

(a) (b)

(c) (d)

Figure 4.17: (a) Longitudinal image of anodized AlF3-450 after annealing at 150C for 30 minutes at 25X magnification. (b) Longitudinal image of anodized AlF3-450 after annealing at 150C for 30 minutes at 200X magnification. (c) Longitudinal image of anodized AlF3-450 after annealing at 500C for 30 minutes at 25X magnification. (d) Longitudinal image of anodized AlF3-450 after annealing at 500C for 30 minutes at 200X magnification.

The resulting microstructure of anodized screw extruded aluminium foil based 500°C 3mm wire after annealing is presented in figure 4.18. The magnification is 25X for (a) and (c), with 200X magnification for b) and d). There is minimal change in structure after annealing also for this sample. In image (d) the particles seem larger than previous, but they are still too small to be accurately quantified in terms of size.

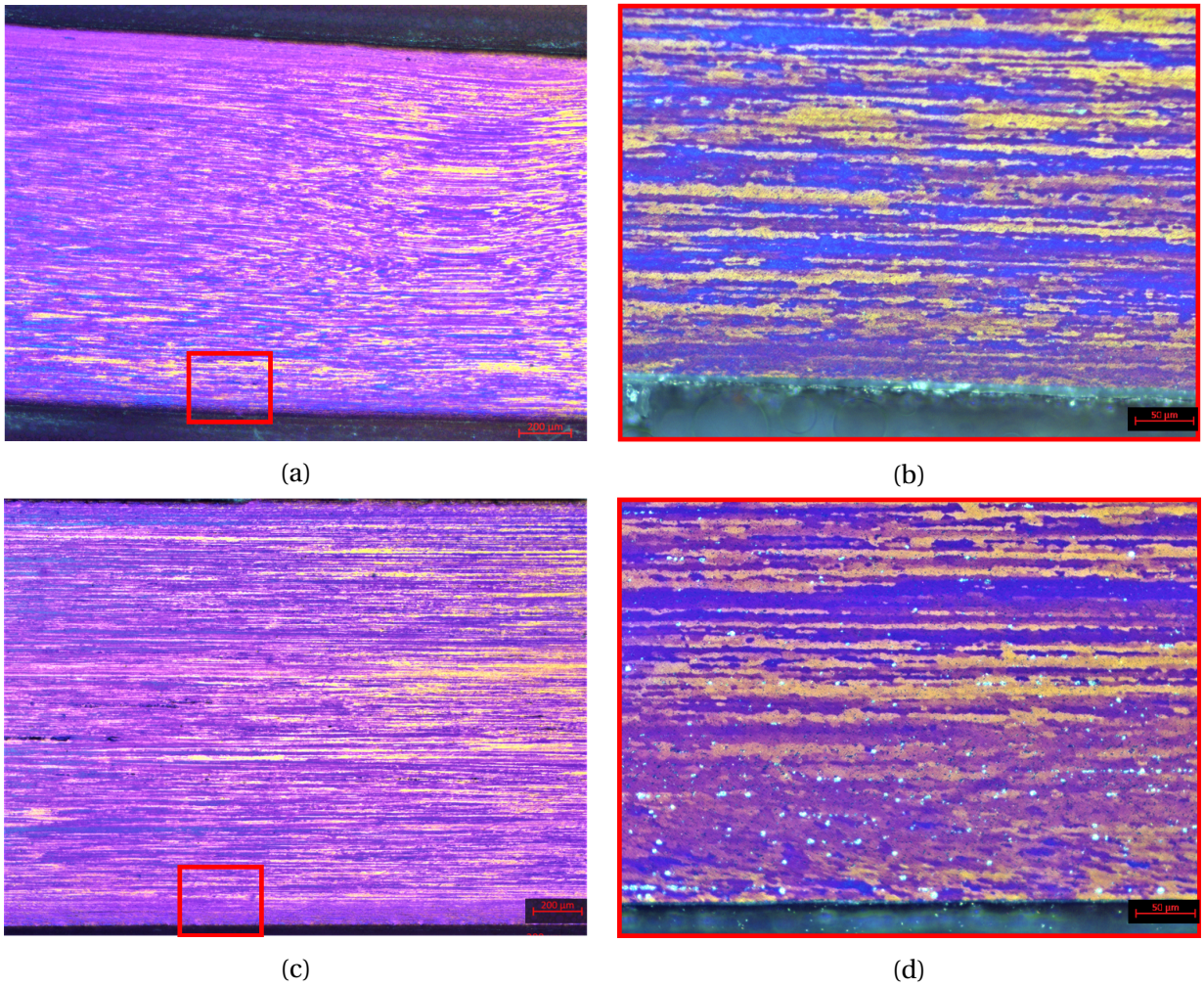

(a) (b)

(c) (d)

Figure 4.18: (a) Longitudinal image of anodized AlF3-500 after annealing at 150C for 30 minutes at 25X magnification. (b) Longitudinal image of anodized AlF3-500 after annealing at 150C for 30 minutes at 200X magnification. (c) Longitudinal image of anodized AlF3-500 after annealing at 500C for 30 minutes at 25X magnification. (d) Longitudinal image of anodized AlF3-500 after annealing at 500C for 30 minutes at 200X magnification.

4.2.7 Density

The density measured by pycnometer and contrast area mapping is described in table 4.2. The contrast area mapping is done using iSolution DT software. The density is here about 97.5% measured by a pycnometer, showing varying results for image mapping for the SEM and OM images. The pycnometer measures the density for the entire sample, while OM and SEM measures for a selected section of the sample.

Table 4.2: Density of AlF3 using different techniques. OM = Optical Microscope and SEM = Scanning electron microscope.

Method	Density [g/cm^3]	Percent of theoretical
Theoretical density	2,7843	100%
Pycnometer	2.702	97.44%
OM contrast	2.669	95.86%
SEM contrast	2.7648	99.3%

4.3 Screw extruded aluminium foil based 10mm profile

4.3.1 Hardness

The hardness for screw extruded aluminium foil based 10mm profile is presented in figure 4.3. The hardness is measured in Vickers hardness. The results show a low change in hardness for a change in extrusion temperature from 450°C to 490°C. The difference is outside the standard deviation, and is the highest for AlF10-450.

Table 4.3: Average hardness values in Vickers hardness for AlF10 samples. Standard deviation also included.

Sample	Avg. Hardness [HV]	Std. Dev
AlF10-450	36,8	0,837
AlF10-490	37,4	0,548

4.3.2 Tensile strength

The tensile tests done on screw extruded aluminium foil based 10mm profile is presented in figure 4.19. The extrusion(die) temperature was 450°C. The tests show a stable yield strength of 70 MPa and a stable ultimate tensile strength of 120 MPa. The fracture-strain is within 37-43% elongation.

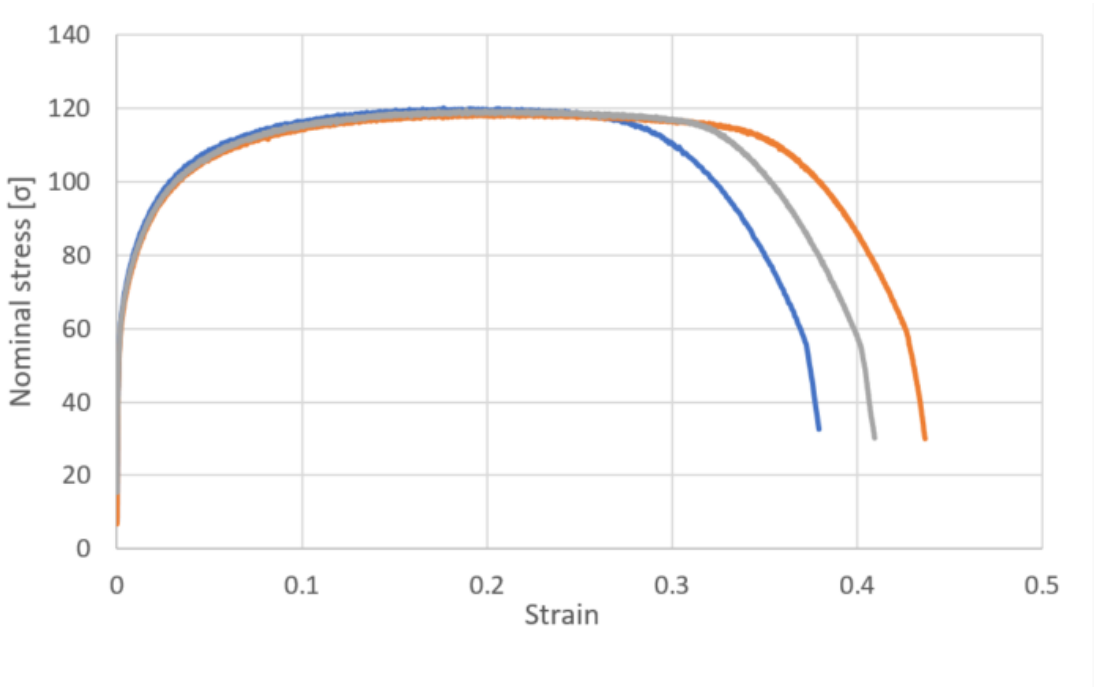

Figure 4.19: Tensile tests for AlF10-450. The tests are parallels.

The tensile tests done on screw extruded aluminium foil based 10mm profile is presented in figure 4.20. The extrusion(die) temperature was 490°C. The tests show a stable yield strength of 70 MPa and two samples shows an ultimate tensile strength of 115 MPa. One sample deviates severely from the other samples, with an ultimate tensile strength (UTS) of 150 MPa before fracturing rapidly. The tensile curve for the deviating material is very dissimilar to its parallels, and to the three tested samples at 450°C.

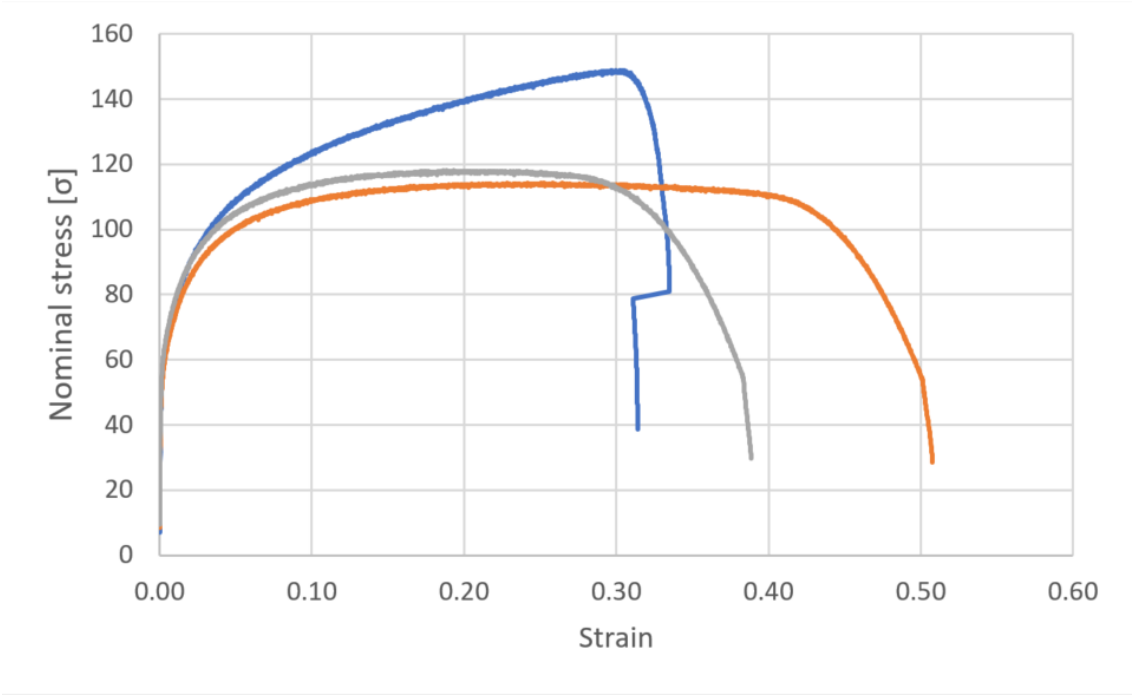

Figure 4.20: Tensile tests for AlF10-490. The tests are parallels.

4.3.3 Fractography

The deviating tensile tested AlF10-490 sample was investigated in SEM to determine the fracture type, and compared to a successful tensile tested AlF10-490 sample. Figure 4.21 shows the fracture surfaces. The images show dimple formation in the shear fractured part at the side for the deviating sample as seen in (c). The centre of the deviating tensile test contained a deep hole in the centre with an unusual structure. The structure is shown in (e) and (f) at 200X magnification and 5000X magnification. The normal sample shows dimple formation as seen in (b) and (d).

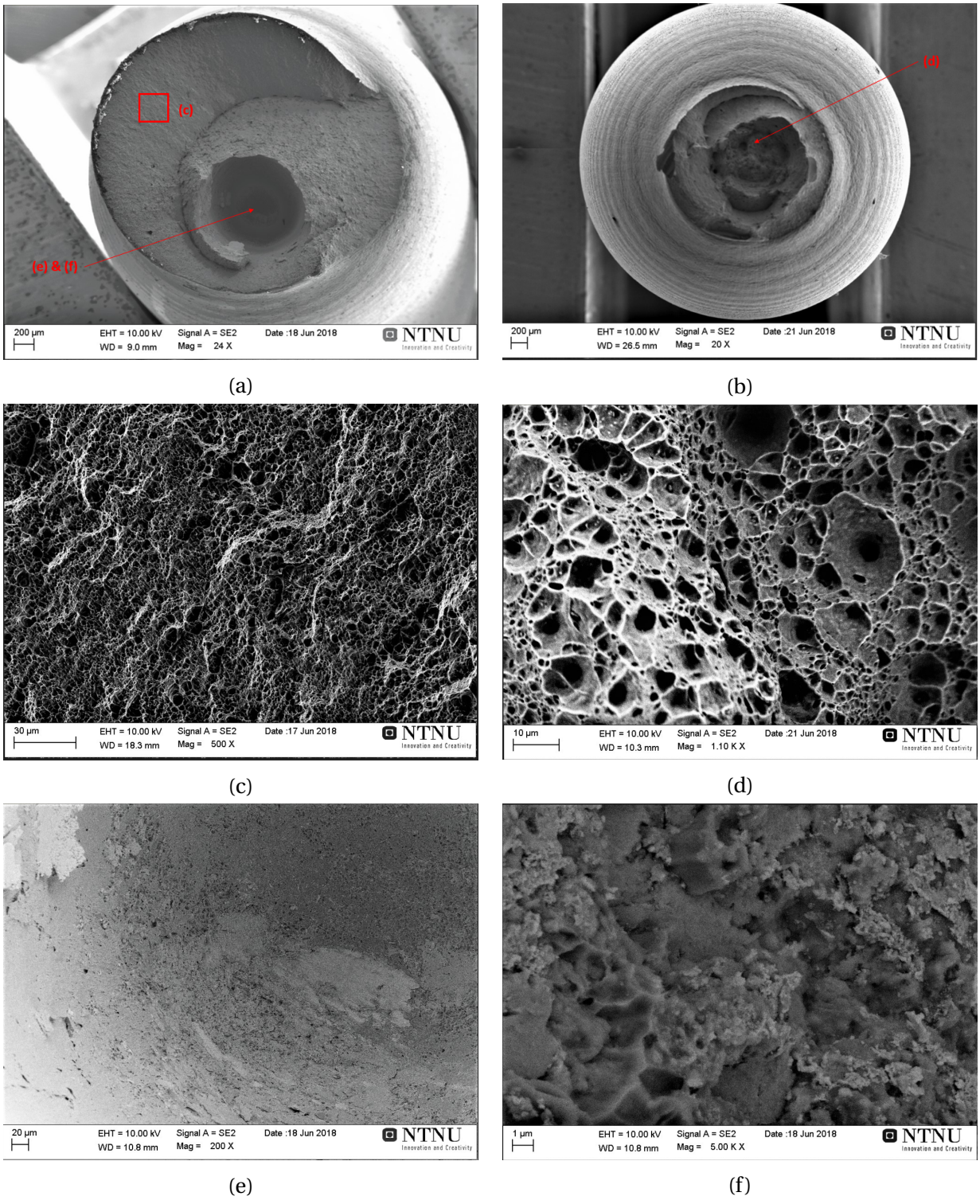

Figure 4.21: (a) Macroscopic SEM-image of fracture surface for deviating tensile tested AlF10-490. (b) Macroscopic SEM-image of fracture surface for normal tensile tested AlF10-490. (c) SEM-image of fracture surface side showing elongated dimples for deviating tensile tested AlF10-490. (d) SEM-image of fracture surface centre showing dimples with small particles in some. (e) Additional SEM-image of fracture surface for deviating tensile tested AlF10-490. (f) Additional SEM-image of fracture surface for deviating tensile tested AlF10-490.

4.3.4 Microscopy

The resulting microstructure of anodized screw extruded aluminium foil 450°C 10mm profile is presented in figure 4.22. The magnification is 25X for (a) and (c), with 100X magnification for b) and d). Due to long anodizing time and high iron content, some corrosion occurred that caused black spots on (a). The microstructure contains small grains and a fibrous structure.

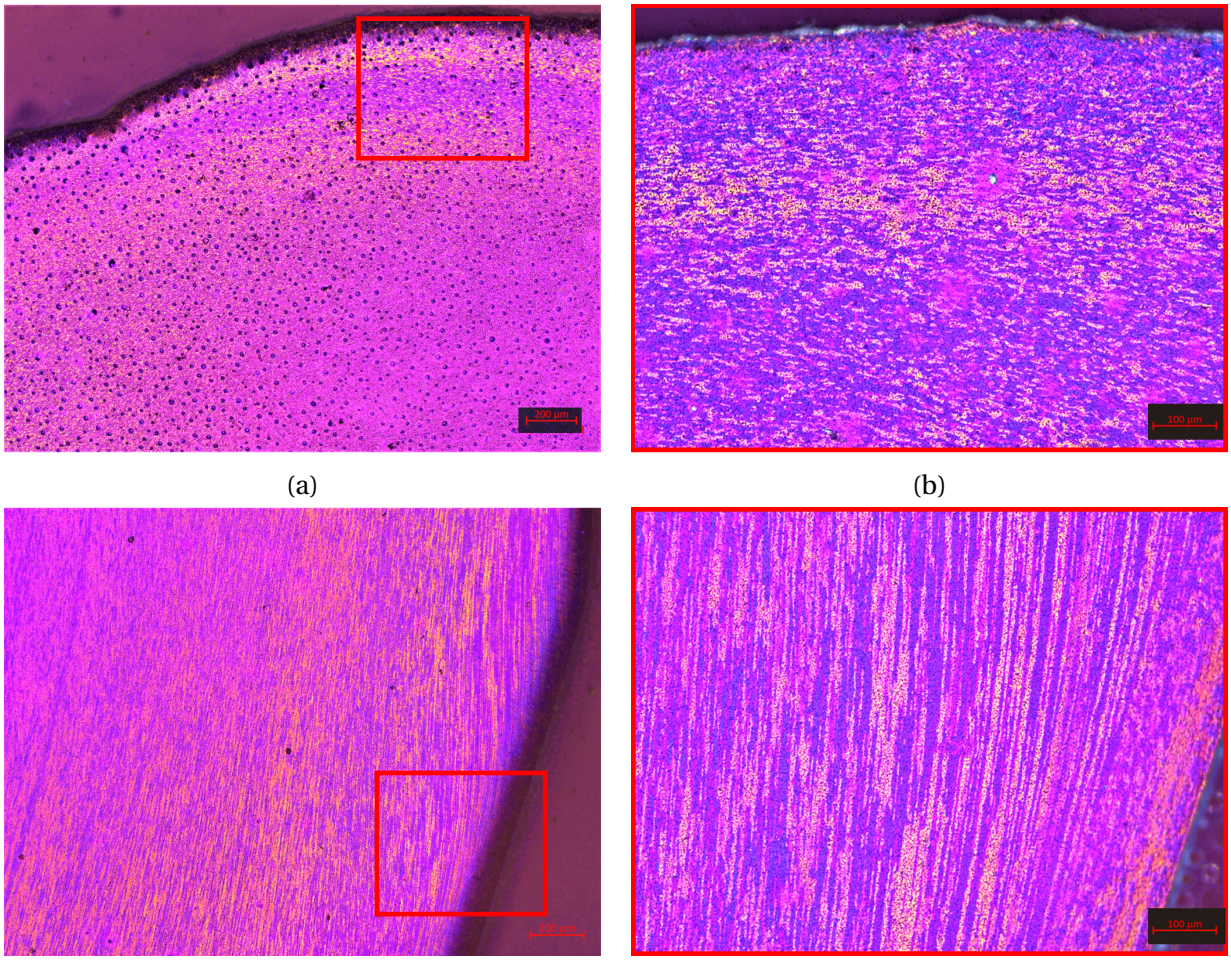

(a) (b)

(c) (d)

Figure 4.22: (a) Cross-sectional image of anodized AlF10-450 at 25X magnification. (b) Cross-sectional image of anodized AlF10-450 at 100X magnification. (c) Longitudinal image of anodized AlF10-450 at 25X magnification. (d) Longitudinal image of anodized AlF10-450. at 100X magnification.

The resulting microstructure of anodized screw extruded aluminium foil 490°C 10mm profile is presented in figure 4.23. The magnification is 25X for (a) and (c), with 100X magnification for b) and d). Due to long anodization time and high iron content, some corrosion occurred, causing black spots on (c). The results are very similar to AlF 3mm and AlF 10mm 450C. The structure is very fine-grained, and fibrous.

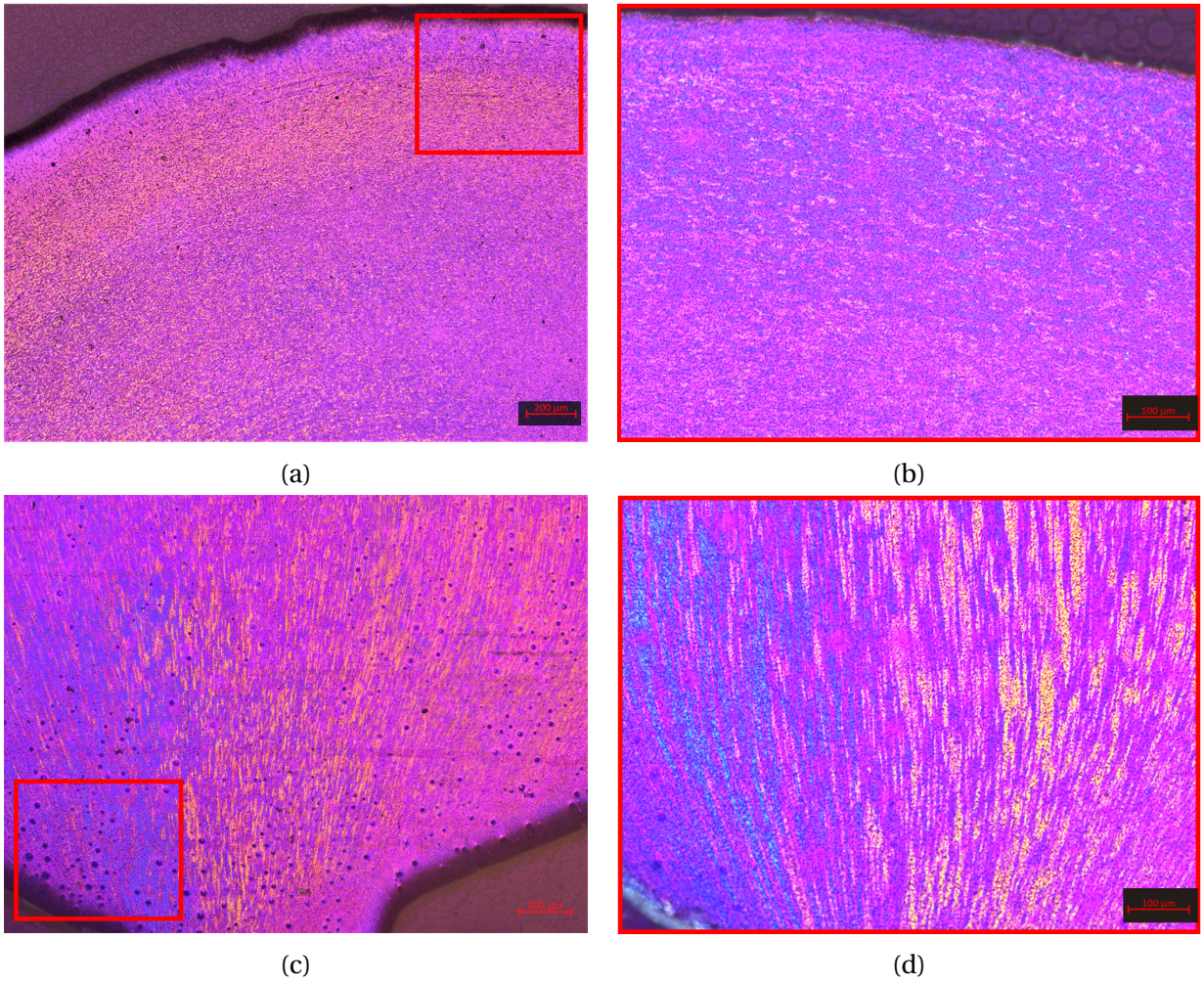

(a) (b)

(c) (d)

Figure 4.23: (a) Cross-sectional image of anodized AlF10-490 at 25X magnification. (b) Cross-sectional image of anodized AlF10-490 at 100X magnification. (c) Longitudinal image of anodized AlF10-490 at 25X magnification. (d) Longitudinal image of anodized AlF10-490 at 100X magnification.

4.3.5 Particle analysis in SEM

A polished sample of AlF10-450 was imaged by SEM to determine the type of the particles and their distribution. Figure 4.24 shows the surface of AlF10-450 at 2000X magnification, with many bright particles on the surface. The size of the particles is around 0.1 to 2μm.

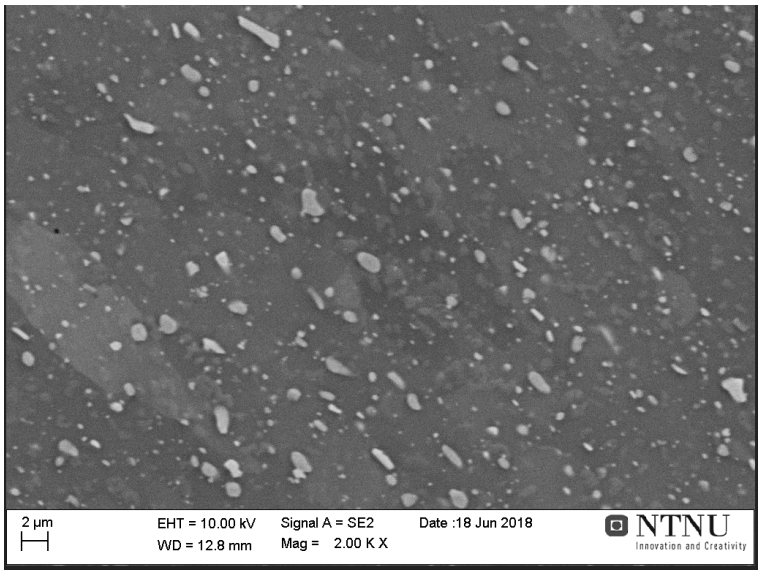

Figure 4.24: Particles on surface of AlF10-450, 2000X magnification.

An EDS analysis was conducted on the particles found on the surface. One analysis can be seen in figure 4.25. The results show that two particle types were discovered. Out of 10 analysed particles 3 were of type 1 (containing iron) and 7 of type 2, showing the same composition as the matrix. Type 1 and Type 2 particle compositions in atomic percent is shown in table 4.4.

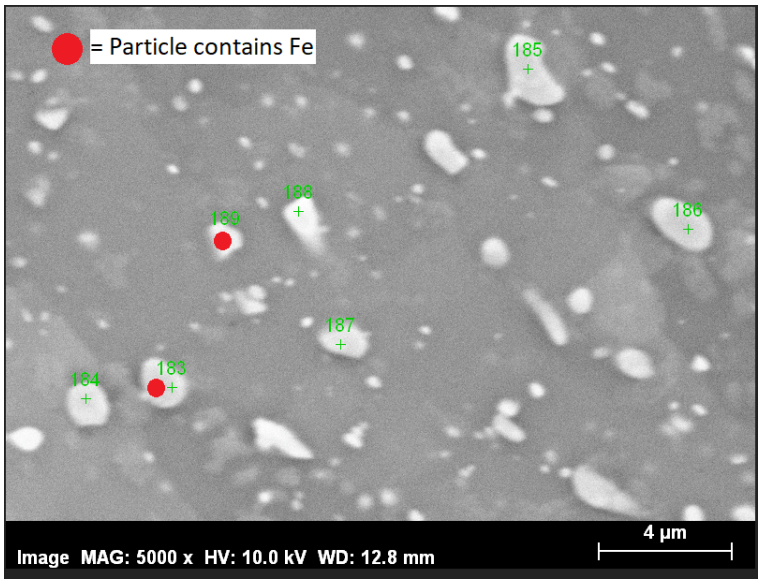

Figure 4.25: 7 particles selected for first EDS element analysis.

Table 4.4: My caption

Element [at%]	Particle type 1	Particle type 2	Surface (matrix)
Al	72.4	89.5	88.1
Fe	8.8	0	0
C	12.1	8.2	9.3
O	1.5	1.1	1.2
Mg	0.9	0.9	0.8
Mn	2.4	0	0.1

4.3.6 Density

The density measured by pycnometer and contrast area mapping is described in table 4.5. The density is about 98% from the pycnometer measurement. This measurement combined material from both AlF10-450 and AlF10-490 to measure the density.

Table 4.5: Density of AlF10 using different techniques. SEM = Scanning electron microscope.

Method	Density [g/cm^3]	Percent of theoretical
Theoretical density	2,7943	100%
Pycnometer	2,7392	98.03%
OM contrast	2,7496	98.4%

5 Discussion

5.1 Electrical conductivity

5.1.1 Calibration

Comparing the measurements done on the reference wires A-D in 1992 by Hydro Sunndalsøra with present measurement conducted in 2018, shows an average difference of measured resistance of 0.6%. This implies that the OM21 apparatus gives comparable results after 26 years.

5.1.2 Effect of screw extrusion process on electrical conductivity

The conductivity of super pure aluminium is referenced in literature to 64.5%IACS[29], 64.95%IACS[17] and 64.944[30]. Previous experimental work done in 1992 by Sintef and Hydro Sunndalsøra gives a calculated conductivity of 65.138%IACS for a Vigeland 3,47mm wire with the OM21 apparatus used in this thesis. The calculated electrical conductivity from OM21 measurements is higher than any reported conductivities earlier,so the OM21 apparatus must show too low resistance. The results are still close to the values listed in literature.

The conductivity of screw extruded 99.99% pure (super pure) aluminium is about 64.9%IACS for all tested specimens. This is only 0.05%IACS away from values given in literature[17][30]. Considering that the OM21 apparatus gives slightly too low resistance, the calculated conductivity of screw extruded wires is slightly too high. The estimated value for a "more correct" conductivity for screw extruded SP-AL is about 64.6%IACS. This assumes that the reference wire should show a conductivity similar to the values given in literature.

The reason for a drop in conductivity for screw extruded wires can be attributed to deformation

induced during screw extrusion[19], oxide formation in the bulk of the material[27] and change in amount of elements in solid solution[15]. If a deformation of 1500% from screw extruding is assumed[31], according to figure 2.7 an increase of resistivity of about 10% should be observed. The difference between the estimated conductivity for screw extruded 99.99% pure aluminium, versus literature values is only 0.5%. This indicates that the deformation is recrystallized as it is being extruded. The effect of oxides, and the amount of alloying elements in solid solution is assumed to be low, as the conductivity is still high after screw extrusion.

5.1.3 Effect of screw extrusion temperature on conductivity

The effect of a die temperature of 220°C versus 320°C is minimal for screw extruded super pure aluminium wires. A bigger temperature difference should be used to easier differentiate the effect of extrusion temperature, with larger parallels to reduce variance within each extrusion temperature. Previous work shows better properties for commercially pure aluminium at 335°C than for 400°C[32].A Study done on equal channel angular extrusion gives a lower grain size for a lower extrusion temperature[33]. As precipitation of iron and recrystallization for 1xxx commercially pure aluminium occurs around 450°C[15], a change in properties could occur around this temperature. The reason that the low extrusion temperature (220°C) for SP-Al is possible is due to the low flow stress of the material.

5.1.4 Effect of annealing screw extruded super pure aluminium 3mm wire

The evolution of electrical conductivity as seen in figure 4.2 shows a decrease in electrical conductivity for different annealing compared to as-extruded. This trend is also found in[15] and partly in[32]. Due to the deformation induced by screw extrusion one could expect an increase in conductivity after annealing due to dislocation termination[19], however the experimental results do not support this. The reason for the reduction in conductivity is not known, but the amount of alloying elements in solid solution is believed by the author to play a role in this.

5.1.5 Electrical conductivity of screw extruded aluminium foil based 3mm wire

The conductivity of screw extruded aluminium foil based 3mm wire described in figure 4.10 varies substantially, from 56%IACS to 57.8%IACS. The two different samples for each die temperature are not consistent neither. The difference could indicate microstructural variance or variance in composition for the screw extruded wire along its length.

The reduced electrical conductivity compared to super pure aluminium is largely due to the high iron content (1.24 wt%) as seen in table 3.3. The calculated conductivity based on figure 2.9 gives a value of 57.18%IACS which matches the experimental results.

The evolution of electrical conductivity does not show any clear trends. Figure 4.11 shows that a die temperature of 500°C gives a higher conductivity, but this drops with annealing at 500°C for 30 minutes. As the results after annealing at 500°C are the same, this could mean they are structurally more similar now. The microscopical images does not reflect a change in microstructure for either of the extrusion temperatures after annealing.

5.2 Variation in cross-sectional area

Calculating the conductivity using equation 2.4 for screw extruded super pure aluminium wires gives consistent results compared to averaging the cross-sectional area of the wire. Screw extruded wires does not give an uniform thickness using neither single flight screws[32] nor double flight screws. The cold drawn reference wires all uniformly measure a diameter of 3,47mm. Therefore the result calculated by the density method matches the result calculated by the area much better as seen in Ref. Vigeland Al in figure 4.1. If uniform thickness is required for applications of screw extruded wires, cold drawing the wires after screw extrusion could be attempted. This could also enhance mechanical properties[34]. Due to the uneven surface of single flight screw extruded profiles, a double flight screw extruded wire would be more fit to be cold drawn.

5.3 Mechanical properties of screw extruded aluminium

5.3.1 Hardness

The hardness after different processing steps as presented in figure 4.3 shows that screw extrusion greatly increases hardness from feedstock. Annealing at 150°C gives a slight increase in hardness, however this is well within the standard deviation. The hardness is reduced after annealing at 500°C, likely due to recrystallization and grain growth as can be seen in figure 4.5.

The hardness of screw extruded aluminium foil based 3mm wire as presented in figure 4.12 shows a large difference between an extrusion(die) temperature of 450°C and 500°C. The hardness is higher for the 500°C screw extruded sample for all stages. The microstructure as seen in figure 4.15 and figure 4.16 does not show large differences, and this points to recrystallization not being present. Due to the high concentration of iron, concurrent precipitation will delay recrystallization by a large factor. An increased temperature could allow more iron to go into solid-solution, giving a strength contribution. This would however reduce the electrical conductivity[15], but it is not shown clearly in figure 4.10.

The hardness of the screw extruded aluminium foil based 10mm profile with an extrusion temperature of 450°C and 490°C is within/ very close to the standard deviation of each other. This indicates that a difference in screw extrusion temperature of 40°C does not affect the hardness much. Compared to the screw extruded aluminium foil based 3mm wire, the hardness is similar. As the chemical compositions and extrusion temperature ranges are relatively close, this is expected. The large standard deviations and variances between wires indicates that the hardness varies due to other factors such as pores and an inhomogeneous particle distribution.

5.3.2 Tensile testing

The tensile tests for screw extruded super pure aluminium 3mm wire gives consistent values for they yield strength and UTS. The strain varies significantly, from about 0.20 to 0.55. An expla-

nation could be stress localization, where stress is concentrated at inhomogeneities or pores in the structure, causing an early fracture in screw extruded products.

The tensile tested screw extruded aluminium foil based 3mm wire shown in figure 4.13 gives very similar results for all parallels. The results are also similar to the tensile tests for AlF10. The tensile tests for screw extruded aluminium foil based 10mm profile as seen in figures 4.19 and 4.20 shows similar results for the yield strength and UTS. The last 490°C specimen deviates from all other, and shows a much larger UTS, about 150MPa. The increased UTS of 150MPa was only found in 1 out of 6 tensile tested AlF 10mm, and 0 out of 2 successfully tensile tested AlF 3mm. This indicates a deviation that is not commonly occurring.

5.4 Behaviour of screw extruded aluminium foil based wire and profile during fracture

The fracture as seen in figure 4.14 shows indications of mainly microvoid coalescence with dimple formation. The circular pattern in figure 4.14 (a) could make the material more anisotropic compared to conventional extrusion techniques.

The SEM-images in figure 4.21 shows that the normal AlF10-490 tensile tested sample has a ductile fracture with microvoid coalescence and dimple formation. The deviating contains dimple formation at the side cup, with an unknown fracture surface down in the large hole in the centre. Comparing the fracture surface seen in figure 4.21 (f) to an Al-Al_2O_3 Metal Matrix Composite(MMC) fracture as seen in figure 5.1 shows some similarities. However more evidence for alumina particles being the cause of the fracture is needed to draw a clear conclusion. If an element analysis could be conducted at the fracture surface, this could indicate if oxygen is present. The deviating sample displays a problem for screw extruded products, where inclusions or inhomogeneous particle distributions can occur. As screw extrusion is still in the research stage, these problems can be further investigated before commercialization of the process.

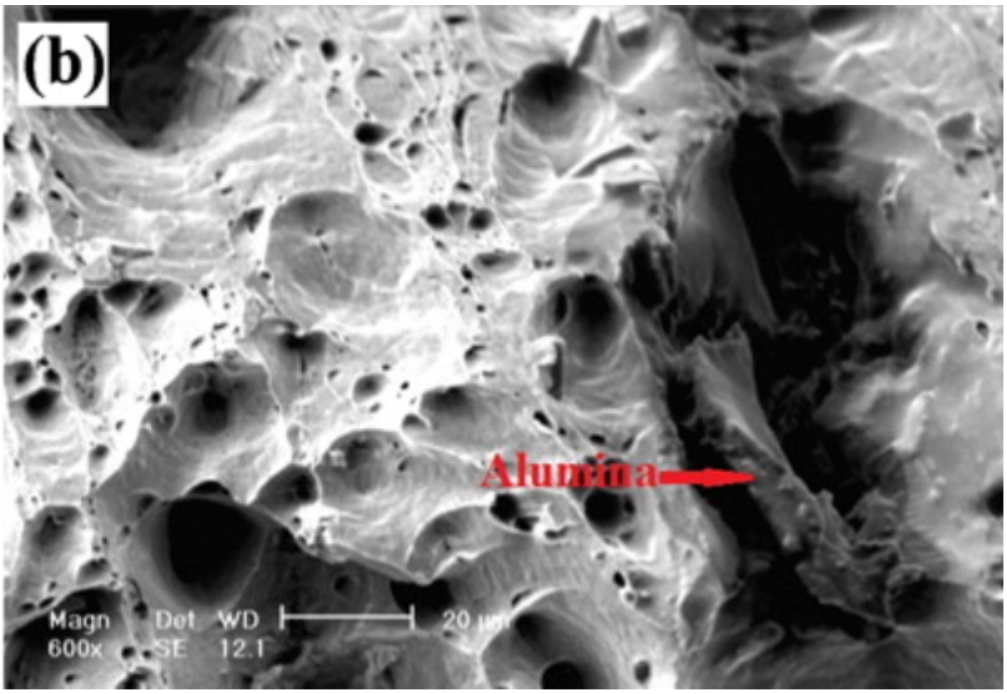

Figure 5.1: Fracture image in SEM for an Al-Al_2O_3 MMC showing Al_2O_3 at the fracture surface. From [35].

5.4.1 Particle analysis in SEM

The particles found in the EDS analysis for AlF10 consists of two types, one containing iron and one with equal composition as the surface. It is very unlikely that the composition is the same for the surface and the particles, so this is more likely a problem with the EDS measurements. Due to the emission volume of the electron beam it is not able to pick up particles with a size lower than about 1μm. Because of this, other techniques such as TEM or XRF could be used to better characterize the particles. Research conducted by Skorpen, Roven, and Reiso shows that oxide particles in screw extruded aluminium can be seen using TEM[36]. The natural oxide layer thickness is only a few nanometres, so these are not measurable by SEM.

5.5 Electrical conductivity and mechanical properties of screw extruded wires compared to commercial alternatives.

Selected properties of screw extruded wires and comparable alternatives found in literature is presented in table 5.1. The 1199 alloy found in literature is the same purity as the screw extruded SP-Al, and 6101-T61 is a common electrical conductor alloy with the same conductivity as the screw extruded AlF3.

Table 5.1: Comparison of screw extruded wires with alloys produced by conventional techniques. The AA1199-O Alloy is from[17], where O means un-tempered state and the AA6101-T61 alloy is from[37]. *As ASTM E-140 does not give conversion rates from HB to HV under HB values of 44, the ratio at the lowest conversion rate is used (HV=HB * 1.2).

Name	Electrical conductivity [%IACS]	Hardness [HV]	Tensile strength [MPa]	Ultimate tensile strength [MPa]
SP-Al-220	64.90	19.4	35	43
SP-Al-320	64.92	21.4	35	43
AA1199-O	64.5	19*	15	50
AlF3-450	56.75	33.8	65	110
AlF3-500	56.80	38.4	65	110
AA6101-T61	57	X	100	140

Comparing the hardness of the screw extruded Super pure aluminium to an AA1199 alloy (99.99% pure aluminium alloy), the hardness of screw extruded super pure aluminium is about equal for SP-Al-220 versus the un-tempered state of AA1199. SP-Al-320 is about 10% harder than the un-tempered state of AA1199. If the AA1199 alloy is tempered to H18, the hardness increases to 33HV*. (*As ASTM E-140 does not give conversion rates from HB to HV under HB values of 40, the ratio at the lowest conversion rate is used (HV=HB * 1.2).) The hardness of the AA6101 alloy was not given.

The yield strength and UTS of an AA1199 alloy can be seen in figure 4.4 as a function of purity. Comparing the yield strength and ultimate tensile strength of screw extruded super pure aluminium to an AA1199 alloy we see that the yield strength is larger for the screw extruded wires (30 MPa vs 15MPa) and the UTS is lower for the screw extruded wires (44MPa vs 50 MPa). The

tempering state for the 1199 alloy is not known in figure 5.2.

For the aluminium foil the two successful specimens gives very similar results. Comparing a screw extruded aluminium foil based profile to an AA6101 alloy gives a lower yield strength for the screw extruded wire (70MPa vs 100MPa) and a lower UTS (110 MPa vs 140MPa).

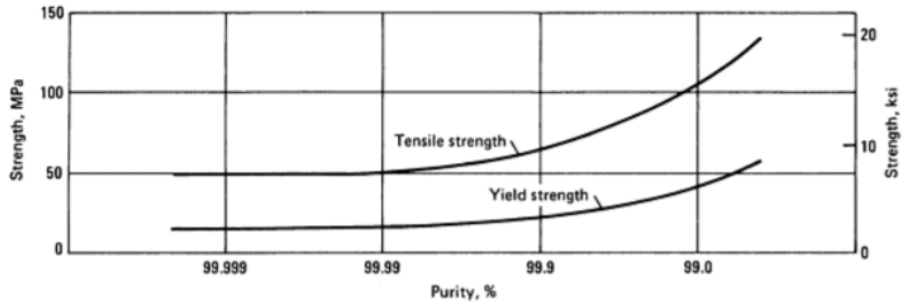

Figure 5.2: Tensile strength for different purities of unalloyed Aluminium.

5.6 Screw extrusion as a compacting technique

5.6.1 Chemical composition change for super pure aluminium

The change in chemical composition for super pure aluminium from as-received blocks to screw extrusion screw-tip can be seen in table 5.2. This shows a reduction in purity of 0.015%. This is before the largest compacting occurs at the die, so even more contamination could occur for screw extruded profiles. The contamination is mostly iron, which increases from 0 to 0.01%. As the screw, chamber and dies are all made from tool steel this could be a potential source of contamination. The chemical analysis did not check for carbon, which is another element that is found in the steel made die, container and screw[38].

Table 5.2: Change in chemical composition from as-received blocks of super pure aluminium to screw extruded super pure aluminium, as measured by the material plug in front of the screw tip.

Element	Change [wt%]	Element	Change [wt%]	Element	Change [wt%]
Al	0.0154	Ti	0.00024	Ca	0.00047
Si	-0.00166	Cr	0.00043	B	0.00006
Fe	0.01042	P	0.00003	Ag	0
Cu	0.00046	Ni	0.00031	Co	0.00001
Mg	0.00048	Pb	0.00002	Zr	0.00002
Zn	0.00009	Sn	0.00002		
Mn	0.00072	Na	0.00001		

5.6.2 Density

The density seems to lie between 95.8% and 99% for all samples, and the same density is also measured for previous studies[32]. As the pycnometer measures the density for the entire sample, while image contrast measurements only cover a portion of the sample, the pycnometer measurements should be more accurate. The results indicate that the density is higher in the super pure aluminium, while the increased alloying content or higher extrusion temperature decreases the density for the screw extruded aluminium foil. The image contrast measurement indicate that there are local variations in density in the sample, i.e. that the porosities are not homogeneously distributed. Previous studies point to that the cleanliness of the feedstock[28] for screw extrusion and the extrusion ratio for hot extrusion of scrap[39] affects the density. These aspects should also be considered when evaluating the need of a high-density product. Compared to other compacting techniques such as Briquetting[40] that gives a density of 65% of theoretical density, the density of screw extruded profiles is superior.

6 | Conclusion

This study has assessed two possible applications of screw extruded products; (i) electrically conducting wires, and (ii) as a compacting technique for aluminium scrap. The mechanical properties and electrical conductivities are measured and compared to alloys produced using existing methods. The key findings are presented as follows:

- The screw extrusion process does not significantly affect the conductivity of a super pure aluminium wire. The values measured for the screw extruded super pure (99.99% pure) aluminium wire closely matches values given in literature for electrical conductivity of 99.99% pure aluminium.
- Screw extrusion of clean commercial aluminium foil gives a metal-bonded product with high density and adequate mechanical properties. The material fractures in a ductile manner. Screw extrusion as a compacting process displays promising results for aluminium foils. This can ease recycling of materials that are difficult to recycle today.
- The screw extrusion process introduces some contamination in the produced material. The main element introduced is iron, this is most likely due to the screw extruder container, screw and die are all made from steel.
- Annealing of screw extruded wires at 500°C or 150°C for 30 minutes does not improve electrical conductivity in this study. After the material recrystallizes the conductivity should increase due to less deformation, however the experimental results do not support this. The reason for the reduced electrical conductivity is not known, and should be further investigated.

7 Future work

Based on the results given by this thesis and results given in literature, two suggestions to further study are presented as follows:

- Evaluate if screw extruded wires can be cold drawn after screw extrusion to further increase mechanical properties, with a limited decrease in electrical conductivity. This could possibly optimize the relationship between electrical conductivity and mechanical properties[15].
- Attempt compacting industrial foil/thin sheet waste according to different foil scrap grades[10]. Both contaminated and clean foils should be experimentally tested to further investigate if screw extrusion could provide an environmentally friendly way to recycle commercial foil scrap.

Bibliography

[1] S Das and W Yin. “The worldwide aluminum economy: The current state of the industry”. In: *JOM* 59.11 (2007), pp. 57–63. ISSN: 1047-4838.

[2] J C Werenskiold et al. “Screw extruder for continous extrusion of materials with high viscosity”. U.S. pat. EP 2 086 697 B1. May 1, 2013.

[3] D Meulenbroeks. *Aluminum versus Copper Conductors*. White paper. Siemens Center of Competence Data Centers, The Netherlands, 2014.

[4] A Kvithyld. *Personal communication with Anne Kvithyld [Figure reprinted with permission from Professor Ray Peterson from TMS 2018]*. 2018.

[5] J R Duflou et al. “Environmental assessment of solid state recycling routes for aluminium alloys: Can solid state processes significantly reduce the environmental impact of aluminium recycling?” In: *CIRP Annals* 64.1 (2015), pp. 37–40. ISSN: 0007-8506.

[6] J Cui. “Solid state recycling of aluminium scrap and dross characterization”. PhD thesis. NTNU, 2011.

[7] Sustainable Minds. *Learn about SM Single Score results*. 2018. URL: http://www.sustainableminds.com/showroom/shared/learn-single-score.html (visited on 06/09/2018).

[8] *Workshop on Aluminium Recycling*. 2010.

[9] Fortum AS. *Facts about combustion process [In norwegian]*. 2018. URL: https://www.fortum.no/fakta-om-forbrenningsprosessen (visited on 06/07/2018).

[10] Inc. Institute of Scrap Recycling Industries. *Scrap sepcifications circular 2018*. Tech. rep. Institute of Scrap Recycling Industries, Inc., 2018.

[11] H Valberg. *Applied metal forming: Including FEM analysis*. 2010. ISBN: 978-0-521-51823-9.

[12] J Evertsson et al. “The thickness of native oxides on aluminum alloys and single crystals”. In: *Applied Surface Science* 349 (2015), pp. 826–832. ISSN: 0169-4332.

[13] K Wefers and C Misra. *Oxides and Hydroxides of Aluminum*. Tech. rep. Alcoa Laboratories, 1987.

[14] M S Hunter and P Fowle. "Natural and Thermally Formed Oxide Films on Aluminum". In: *Journal of the Electrochemical Society* 103.9 (1956), pp. 482–485. ISSN: 00134651.

[15] G Langelandsvik. "Optimization of electrical conductivity in screw extruded wires". MA thesis. NTNU, 2017.

[16] *Copper wire tables*. 1914.

[17] *Aluminum and aluminum alloys*. ASM specialty handbook. ASM International, 1993. ISBN: 087170496X.

[18] R E Hummel. *Electronic Properties of Materials*. 2011, p. 488. ISBN: 978-1-4419-8164-6.

[19] J Schrank et al. "Effect of high deformation of electrical resistivity in pure aluminium." In: *Scripta metallurgica* 14.10 (1980), pp. 1125–1128. ISSN: 00369748.

[20] R S Seth and S B Woods. "Electrical resistivity and deviations from Matthiessen's Rule in dilute alloys of aluminum, cadmium, silver, and magnesium". In: *Physical Review B* 2.8 (1970), pp. 2961–2972. ISSN: 01631829.

[21] A S Karolik and A A Luhvich. "Calculation of electrical resistivity produced by dislocations and grain boundaries in metals". In: *Journal of Physics: Condensed Matter* 6.4 (1994), p. 873.

[22] S Karabay. "Modification of AA-6201 alloy for manufacturing of high conductivity and extra high conductivity wires with property of high tensile stress after artificial aging heat treatment for all-aluminium alloy conductors". eng. In: *Materials and Design* 27.10 (2006), pp. 821–832. ISSN: 0261-3069.

[23] P Guyot and L Cottignies. "Precipitation kinetics, mechanical strength and electrical conductivity of AlZnMgCu alloys". In: *Acta Materialia* 44.10 (1996), pp. 4161–4167. ISSN: 1359-6454.

[24] F J Humphreys. *Recrystallization and related annealing phenomena*. 3rd ed. 2017.

[25] R K Rajat. *Recrystallization Behavior of Commercial Purity Aluminium Alloys*. 2014. DOI: 10.5772/58385.

[26] J Morris and W Liu. “Al alloys: The influence of concurrent precipitation on recrystallization behavior, kinetics, and texture”. In: *JOM* 57.11 (2005), pp. 44–47. ISSN: 1047-4838.

[27] F Widerøe and T Welo. “Using contrast material techniques to determine metal flow in screw extrusion of aluminium”. In: *Journal of Materials Processing Technology* 213.7 (2013), pp. 1007–1018. ISSN: 0924-0136.

[28] A Bilsbak. “Mikrostruktur og mekaniske egenskaper for skrueekstrudert aluminium [In Norwegian]”. MA thesis. NTNU, 2012.

[29] *Metals handbook : 2 : Properties and selection : nonferrous alloys and special-purpose materials*. 10th ed. Vol. 2. ASM International, 1990. ISBN: 0871703785.

[30] Espi Metals. *Aluminum*. 2018. URL: http://www.espimetals.com/index.php/online-catalog/824-Aluminum (visited on 06/17/2018).

[31] K G Skorpen, H J Roven, and O Reiso. “A physical based empirical model for the accumulated strain in noveml Metal Continous Screw Extrusion (MCSE)”. In: *Unpublished* (2018).

[32] M S Vaernes. “Optimization of electrical and mechanical properties for Aluminium conductors”. In: *Internal report for course at NTNU* (2017). Specialization project.

[33] Y C Chen et al. “The effect of extrusion temperature on the development of deformation microstructures in 5052 aluminium alloy processed by equal channel angular extrusion”. In: *Acta Materialia* 51.7 (2003), pp. 2005–2015.

[34] X M Luo et al. “Microstructural Evolution and Service Performance of Cold-drawn Pure Aluminum Conductor Wires”. In: *Journal of Materials Science Technology* 33.9 (2017), pp. 1039–1043.

[35] R Jamaati and M R Toroghinejad. “Microstructure and mechanical properties of Al/Al2O3 MMC produced by anodising and cold roll bonding”. In: *Materials Science and Technology* 27.11 (2011), pp. 1648–1652.

[36] K G Skorpen, H J Roven, and O Reiso. “Comparison of binary AlMg alloys processed by continous screw extrusion or conventional ram extrusion”. In: *Unpublished* (2018).

[37] *Alloy 6101*. Hydro Extruded solutions, 2017. URL: https://www.hydroextrusions.com/contentassets/7a0f14a8e10a42d0b2ad96f818fe1c25/data_sheet_6101_new_metric_08_21_2017.pdf.

[38] Uddeholm. *UDDEHOLM ORVAR® SUPREME*. 2018. URL: https://www.uddeholm.com/files/PB_orvar_supreme_english.pdf (visited on 06/26/2018).

[39] W Z Misiolek et al. "High quality extrudates from aluminum chips by new billet compaction and deformation routes". In: *CIRP Annals* 61.1 (2012), pp. 239–242. ISSN: 0007-8506.

[40] G Tucholski. *Chips versus briquettes: How the aluminium industry can effectively and efficiently recycle scrap*. Aluminium 1-2/2013. Ruf US, 2013.

A | Appendices

A.1 A: Calibration of OM21 electrical resistance apparatus

The electrical resistance measurements done using OM21 compared with measurements done in 1992 when the apparatus was initially purchased is presented in table A.1.

Table A.1: Resistance change for reference wires in 1992 and 2018.

Reference	% change	Sintef result (1992) [mΩ]	Avg. Measured in 2018 [mΩ]	Std dev.	Measurements in 2018[mΩ]			
A	0.454545455	0.275	0.27625	0.00050	0.277	0.276	0.276	0.276
B	-0.087565674	0.2855	0.28525	0.00050	0.286	0.285	0.285	0.285
C	-0.877723971	0.3304	0.3275	0.00058	0.327	0.327	0.328	0.328
D	-0.830924855	0.4152	0.41175	0.00050	0.412	0.412	0.412	0.411

A.2 B: Measurements to calculate electrical conductivity

Table A.2 through A.5 provides the measured data to calculate the electrical conductivities presented in this thesis. Equation 2.3 and 2.4 were used to calculate the electrical conductivity. σ is the electrical conductivity, L is the length between the measuring points for the OM21 apparatus. R is the measured resistance from the OM21 apparatus. A is the cross-sectional area of the wire to be tested. l is the length of the wire to be tested, ρ_d is the density of the wire to be tested, and m is the mass of the wire to be tested.

Table A.2: Electrical conductivity based on area before heat treatment.

Parameter	SP-Al-220 #1	SP-Al-220 #2	SP-Al-320 #1	SP-Al-320 #2	Ref. Vigeland Al	AlF3-450 #1	AlF3-450 #2	AlF3-500 #1	AlF3-500 #2
L [mm]	98.45	98.45	98.45	98.45	98.45	98.45	98.45	98.45	98.45
A [mm^2]	6.342144711	6.238419794	6.267968218	6.319845948	9.456900746	6.099018165	6.099018165	6.099018165	6.106315822
R [mΩ]	0.422625	0.42825	0.42425	0.429875	0.27625	0.511	0.49825	0.51325	0.510375
σ [MS/m]	36.73029272	36.85053124	37.0226144	36.23823521	37.68466013	31.58892841	32.39727529	31.45044796	31.58981373
$\delta\sigma$ [MS/m]	0.053265563	0.056631852	0.057013156	0.058026523	0.05930149	0.065474822	0.05373502	0.054105937	0.057941524
σ [%IACS]	63.3280909	63.53539869	63.8320938	62.47971588	64.97355195	54.46366966	55.8573712	54.22491027	54.46519608
$\delta\sigma$ [%IACS]	0.053265563	0.056631852	0.057013156	0.058026523	0.05930149	0.065474822	0.05373502	0.054105937	0.057941524

Table A.3: Electrical conductivity based on length, mass and density before heat treatment.

Parameter	SP-Al-220 #1	SP-Al-220 #2	SP-Al-320 #1	SP-Al-320 #2	Ref. Vigeland Al	AlF3-450 #1	AlF3-450 #2	AlF3-500 #1	AlF3-500 #2
L [mm]	98.45	98.45	98.45	98.45	98.45	98.45	98.45	98.45	98.45
l [mm]	201	200	201	199.5	199	201	201.5	201.5	201
m [g]	3.3568	3.2964	3.3435	3.2747	5.087	3.3175	3.3213	3.21	3.3188
ρ [g/mm^3]	0.0026989	0.0026989	0.0026989	0.0026989	0.0026989	0.002784352	0.002784352	0.002784352	0.002784352
R [mΩ]	0.422625	0.42825	0.42425	0.429875	0.27625	0.511	0.49825	0.51325	0.510375
σ [MS/m]	37.64592051	37.64395385	37.65090266	37.65578496	37.62630451	32.50155063	33.3779372	33.52593631	32.52860499
$\delta\sigma$ [MS/m]	0.11180592	0.11180568	0.11180568	0.111805281	0.111803444	0.111804722	0.111806958	0.111806958	0.11180592
σ [%IACS]	64.90675951	64.90336871	64.91534942	64.92376717	64.8729388	56.03715625	57.54816759	57.80333847	56.08380171
$\delta\sigma$ [%IACS]	0.11180592	0.11180568	0.11180568	0.111805281	0.111803444	0.111804722	0.111806958	0.111806958	0.11180592

Table A.4: Electrical conductivity based on length and density after heat treatment of 150C for 30 minutes.

Parameter	SP-Al-220 #1	SP-Al-320 #1	AlF3-450 #1	AlF3-500 #1
L [mm]	98.45	98.45	98.45	98.45
l [mm]	201	201	201	201.5
m [g]	3.3568	3.3435	3.3175	3.21
ρ [g/mm^3]	0.0026989	0.0026989	0.002784352	0.002784352
R [mΩ]	0.424	0.427	0.514	0.513
σ [MS/m]	37.52383763	37.40842027	32.31185286	33.54227449
$\delta\sigma$ [MS/m]	0.111806958	0.111807197	0.111808236	0.111806958
σ [%IACS]	64.69627178	64.49727633	55.71009114	57.83150774
$\delta\sigma$ [%IACS]	0.111806958	0.111807197	0.111808236	0.111806958

Table A.5: Electrical conductivity based on length and density after heat treatment of 500C for 30 minutes.

Parameter	SP-Al-220 #2	SP-Al-320 #2	AlF3-450 #2	AlF3-500 #2
L [mm]	98.45	98.45	98.45	98.45
l [mm]	200	199.5	201.5	201
m [g]	3.2964	3.2747	3.3213	3.3188
ρ [g/mm^3]	0.0026989	0.0026989	0.002784352	0.002784352
R [mΩ]	0.429375	0.432125	0.511375	0.510875
σ [MS/m]	37.54532341	37.45971781	32.52125585	32.49676882
$\delta\sigma$ [MS/m]	0.11180592	0.111810392	0.111804642	0.111806559
σ [%IACS]	64.73331622	64.58572036	56.07113078	56.02891176
$\delta\sigma$ [%IACS]	0.11180592	0.111810392	0.111804642	0.111806559